On the benefits of a multiscale domain decomposition method to model-order reduction for frictional contact problems

Donald Zeka, Pierre-Alain Guidault, David Néron, Martin Guiton

On the benefits of a multiscale domain decomposition method to model-order reduction for frictional contact problems

D. Zeka[a], P.-A. Guidault[a], D. Néron[a], M. Guiton[b]

[a] *Université Paris-Saclay, CentraleSupélec, ENS Paris-Saclay, CNRS, LMPS - Laboratoire de Mécanique Paris-Saclay, Gif-sur-Yvette, 91190, France*
[b] *IFP Energies nouvelles, Rond-Point de l'échangeur de Solaize - BP 3, Solaize, 69360, France*

Abstract

In this paper, the efficiency of a multiscale strategy based on a domain decomposition method (DDM) for model-order reduction of time-dependent frictional contact problems is presented. The proposed strategy relies on the LArge Time INcrement (LATIN) nonlinear solver combined with model reduction based on the Proper Generalized Decomposition (PGD). The LATIN presents a robust treatment of contact conditions, sharing similarities with augmented Lagrangian approaches, and naturally leads to a mixed DDM. In addition, the global space-time formulation of the method allows PGD-based model reduction to be used during computations, creating and enriching on-the-fly reduced bases per substructure to better track sliding fronts and propagative phenomena. The introduction of a multiscale strategy in the LATIN framework is consistent with the physics of contact problems, in which phenomena with different wavelengths interact: local solutions at contact interfaces presents high gradient effects with a short wavelength compared to the characteristic length of the structure. By taking advantage of this, the coarse scale problem of the strategy enables to capture efficiently the behavior of the problem at the structural level, focusing then on capturing the local contact variations at the contact interfaces. The most important features of the approach are shown comprehensively on a simple one-dimensional frictional contact problem. Then, its robustness and effectiveness are tested on a two-dimensional multibody frictional contact problem with more complex loadings. Guidelines are also given for choosing the parameters of the strategy, in particular those driving the construction of the reduced basis.

Keywords: frictional contact, model-order reduction, domain decomposition, multiscale strategy, LATIN method, PGD.

1. Introduction

The use of high-fidelity numerical solvers in an industrial setting remains limited to this day because of their considerable computational cost, in particular for highly nonlinear finite element analyses of large-scale structures with a large amount of degrees of freedom as well as a large number of time steps. Among them, the simulation of architectured materials with multiple frictional contact interactions subjected to large displacements is probably one of the most challenging problems in structural mechanics [1, 2].

Frictional contact problems are characterized by strong nonlinearities and non-smooth behaviors at the contact interfaces, with several large contact zones which can lead to numerical issues. The classical treatment of frictional contact conditions with usual finite element methods resorts to techniques originating from constrained optimization methods. Among others, one can cite Lagrange multipliers, penalization, or augmented Lagrangian methods. For a wider overview on the topic, one can refer to [3, 4]. However, all these methods may require prohibitive computational costs, especially in an industrial context with time-dependent loadings and parametric studies. Acceleration or parallelization methods are therefore a necessity to address this issue. Acceleration strategies are commonly based on multigrid methods [5, 6, 7], and enable to accelerate the convergence of the problem by cheaply computing corrections on a coarse discretization. Domain decomposition methods (DDM) with or without overlapping subdomains, the latter being the most used nowadays, have also been developed for the parallelization of large-scale problems. Among them, one can cite primal methods, where the unknowns are the interface displacements, dual methods, which instead privilege interface forces, and mixed methods, where both interface displacements and forces are considered

as unknowns. For an overview on non-overlapping primal and dual methods, one can refer to [8]. The Finite Element Tearing and Interconnecting (FETI) dual method [9, 10, 11] is the most widespread approach, where compatibility between neighboring subdomains is ensured by Lagrange multipliers, corresponding to interface forces. Numerical scalability of the method is obtained with the introduction of rigid body modes as a "coarse scale problem" [12]. The coarse scale problem provides a multiscale aspect to DDM methods: a coarse information is spread on the whole structure allowing non-neighboring subdomains to interact, and thus to speed-up the convergence. Numerically scalable FETI-based DDM techniques for frictional contact problems have been presented in [13] with active set method, and in [14, 15] for an augmented Lagrangian approach. Other approaches refer to FETI-DP [16, 17] or T-FETI methods [18]. Mixed DDM strategies also include those based on the LArge Time INcrement (LATIN) nonlinear solver [19]. The mixed nature of the method enables one to deal with different interfaces characterized by different constitutive behaviors with a single resolution method. When the LATIN-based mixed DDM is not equipped with a coarse scale problem, we refer to it as a monoscale DDM [19, 20, 21]. A multiscale version of the LATIN-based mixed DDM, in which a coarse scale problem is introduced, was firstly described in [22] for heterogeneous structures, and for quasistatic contact problems in [23].

Another, and possibly complementary, way to decrease computational cost consists in adopting reduced-order models (ROM) techniques by seeking the solution of the given problem in a reduced-order basis (ROB), whose dimension is much smaller than the size of the original high-dimensional model [24, 25]. ROM methods can be distinguished by the way in which the ROB is constructed. A first family of techniques, named a posteriori methods, involves a training phase, called offline phase, where the full-order problem is solved for some particular time instants or parameter values, generating the so-called snapshots. Snapshots are then used to create a ROB on which to project the full-order equations and obtain a reduced-order model. The most classical way to obtain a ROB from a given set of snapshots is the Proper Orthogonal Decomposition (POD) [26]. The strong point of the method relies in the fact that the number of relevant POD modes is generally much lower than the scale of the full-order problem. Nevertheless, the quality of the ROM is strongly affected by the representativeness of the ROB, especially for highly nonlinear problems. Another approach to obtain a ROB is represented by the Reduced Basis (RB) method, which improves the procedure for the selection of the appropriate snapshots by an efficient error indicator allowing a certified error quality [24, 27]. A second family of ROM techniques consists in seeking the solution of the targeted problem in the span of a consistent ROB progressively built by a dedicated algorithm during the solving stage. This represents the a priori model reduction methods, where no offline training phase is required. To this family belongs the Proper Generalized Decomposition (PGD) [25, 28].

For contact problems, most of pertinent model reduction techniques rest on a posteriori methods, mainly for frictionless parametric problems with a small number of contact interfaces. They cover POD projection-based methods for displacements and contact forces [29], adopting a non-negative matrix factorization for the construction of a positive ROB for the contact forces, and coupled with a greedy algorithm and a robust error indicator with respect to parameter variations. RB methods have also been applied to parametric frictionless contact problems [30], in a generic nonlinear setting where large displacements are assumed. The non-negativity of the contact forces is achieved through a cone-projected greedy algorithm, and the nonlinear constraints are tackled with the Empirical Interpolation Method hyperreduction technique [31]. Enrichment techniques with POD modes for parametric problems have been succesfully used for the simulation of fretting fatigue in [32]. The bottleneck of the a posteriori methods relies in the computation of snapshots [33, 34]. For large-scale problems, this training step can be very costly. Moreover, for problems involving a huge variety of loading conditions and nonlinear phenomena, especially due to frictional contact interactions, a predetermined ROB may not be able to easily and efficiently capture non-regular and propagating multiscale phenomena that occur at contact interfaces: sliding, sticking and separation zones being difficult to follow. For this reason, an a priori approach based on the PGD coupled with the LATIN nonlinear solver [19] may represent a more efficient way to tackle frictional contact problems through a reduced-order model that allows the ROB to be enriched during computations to account for the evolution of frictional contact conditions.

Nevertheless, for specific problems where high accuracy of contact quantities is required, reduced models alone may not guarantee sufficient accuracy while ensuring at the same time a significant decrease in computational cost. As highlighted in [35, 36, 37], frictional contact problems present a multiscale content, with global modes on the structural level and localized modes bringing corrections at the contact interface level. This suggests the idea that proposing a model reduction method with a multiscale approach may be truly beneficial for problems of this type. To the authors' knowledge, one of the few approaches to achieve such a combination is the multiscale LATIN-based

mixed DDM. Indeed, the LATIN method makes it possible to handle frictional contact problems, apply PGD-based model reduction and introduce multiscale aspects in a robust, flexible and efficient framework. However, mention should also be made of [36], where the authors make use of the LATIN method at the microscale and a multigrid scheme on a macroscale with precomputed global SVD modes.

Applied to different contexts (viscoelasticity, homogenization...) in [38, 39, 40, 41, 42], the multiscale LATIN-based mixed DDM with PGD makes it possible to take into account also frictional contact interactions. However, in these previous works, rather short frictional cracks had a more or less limiting effect on the global scale, surrounded by other material nonlinearities. Moreover, it was highlighted, in the case of the application of the strategy without PGD to the delamination of composite structures [43, 44] or fatigue crack propagation [45], the difficulty of taking into account the potential long-wave effects of a debonding cohesive interface or a long crack propagation in the multiscale LATIN-based DDM, without a suitable coarse scale problem. In fact, it has never been highlighted how and to what extent a multiscale approach, in particular one based on domain decomposition, may be helpful in efficiently solving frictional contact problems with a model reduction approach, and this will be the purpose of the article.

In this paper, we follow the findings presented in [35] in the context of the monoscale LATIN-PGD strategy without DDM for frictional contact problems, where the authors suggest the adoption of a multiscale approach, and propose a low-cost downsizing algorithm to control the quality and size of the PGD basis. Here, the goal is to illustrate why the LATIN method combined with PGD and a multiscale mixed DDM approach is robust to tackle model reduction for frictional contact problems, where multiple and large frictional contact interfaces are present, and what are the benefits to combine DDM and a coarse scale with PGD. This will first be illustrated on a one-dimensional frictional contact problem where the contact interface is large and a large sliding front is present. Some strengths and points of improvement of the LATIN-based multiscale mixed DDM method for the model-order reduction of frictional contact problems will be comprehensively presented. Subsequently, a more complex 2D example with more contact interfaces and more complex loads will be proposed to test the potentialities of the approach. The DDM approach allows to create reduced bases per substructure to better track sliding fronts and propagative phenomena, and the multiscale aspect leads to a significant gain in convergence in the early stages, taking advantage of the multiscale nature of the phenomenon itself. PGD is naturally introduced in the LATIN and allows for on-the-fly enrichment of the ROB where and when required to better follow the evolving frictional phenomena. For highly irregular problems such as frictional contact problems, controlling the quality and size of progressively built PGD basis along the LATIN iterations is crucial for the efficiency of the method. Here, we also go on to investigate the necessity and the benefits of the downsizing algorithm proposed in [35] when adapted to the multiscale and DDM contexts.

The paper is organized as follows. First of all, in **Section 2**, prior to going into the details of the strategy, a simple but representative one-dimensional frictional problem and its reference solution obtained with the LATIN method are presented, which will later serve as basis for an explication of the features of the method. Thereafter, the LATIN method, in its monoscale DDM version, is introduced in **Section 3** and is then applied to the test problem. The strengths of the method are highlighted, as well as some specific points related to frictional contact problems that require further improvements. The introduction of PGD in the LATIN scheme is detailed in **Section 4**, and applied to the test problem, with focus on properly controlling the PGD basis size and quality along the iterations. The multiscale strategy is detailed in **Section 5**, as well as the introduction of PGD in the multiscale case. It is then applied to the simple one-dimensional test problem as well as to a more complex two-dimensional multibody frictional contact problem in **Section 6**. Conclusions and perspectives are finally given in **Section 7**.

2. Preliminary results on a simple 1D problem

Before going into the details of the multiscale LATIN-based DDM strategy for model-order reduction, in this section is investigated the reducibility of the displacements and frictional forces of a one-dimensional benchmark problem. The problem consists of a clamped elastic bar subjected to a time-dependent traction loading $F_d(t)$ on the free boundary. The bar is in contact with a frictional interface along its entire length by means of a normal pressure $p(t)$ acting on it (**Figure 1a**). In practice, it is assumed that the bar is always in contact with the frictional surface due to the pressure p considered to be constant.

Concerning the traction loading acting on the bar, two different loadcases are considered (represented in **Figure 1b**). Both of them start with a preloading stage where the value of 1000 N is reached. The loadcase 1 consists in fully unloading the bar after the preloading, while the loadcase 2 consists in performing some small-amplitude

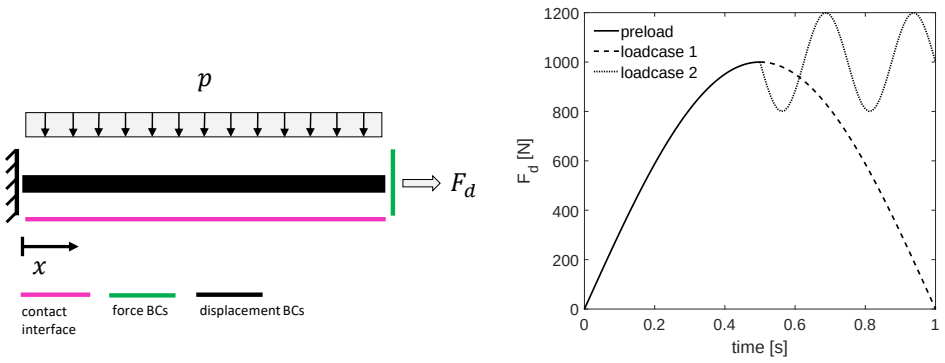

(a) Sketch of the problem.

(b) Time evolution of the different loadcases for F_d.

Figure 1: 1D benchmark problem.

oscillations around this preloaded state. The first loadcase should put us in a more critical condition, since one has to deal with a larger propagation of sliding front which is more challenging to represent with ROM techniques. The parameters adopted for the problem are shown in **Table 1**. The problem, after a finite element discretization in space and time, has been solved with the LATIN method (of which the details will be given in the next section). A converged solution (high number of iterations) was taken as a reference solution and analyzed in the following.

Parameters of the 1D problem	
Young modulus, E	210 GPa
bar cross section, S	3.14 mm^2
bar length, L	1 m
number of DOFs, N_x	50
number of time steps, N_t	100
time interval, $[0, T]$	[0, 1 s]
friction coefficient, f	0.3
pressure load, p	5000 N/m

Table 1: Used parameters for the benchmark problem of **Figure 1**.

In **Figure 2** and **3** are shown, respectively, some time snapshots of the reference solution of the problem for the displacements and frictional contact forces distributions for the loadcase 1. The different gray scales highlight the different sticking-sliding conditions occurring during preloading and unloading in different areas: always sticking conditions in white, sliding-sticking transition in light gray and always sliding in dark gray. The sliding front propagates as the traction force increases, from $t = 0$ s to $t = 0.5$ s during the preloading stage. A portion of the bar, the one closer to the clamped end ($x/L = 0$), remains always in sticking conditions. During the unloading part, another sliding front propagates from the free end of the bar, until the traction force becomes zero. At the end, because of the presence of friction, the bar does not get back to its original undeformed position but remains in a sticking deformed state. In the sticking zone, near the clamped end, the frictional forces are zero, whereas in the sliding zone, during loading, they are equal in absolute value to the Coulomb friction threshold $fp = 1500$ N. In the unloading phase, a new sliding front propagates located in the zone where the friction forces change sign.

After obtaining the reference solution for displacements and frictional forces, an a posteriori Singular Value Decomposition (SVD) [46] analysis can be performed to exemplify the reducibility of the space-time solution. A few SVD space modes for frictional forces are given in **Figure 4**. First modes depict a generally global scale of the solution. One can see that the space modes clearly separate the sticking zone from the ones where sliding occurs. Subsequent space modes still emphasize this distinction as also bring localized corrections to the sliding zones.

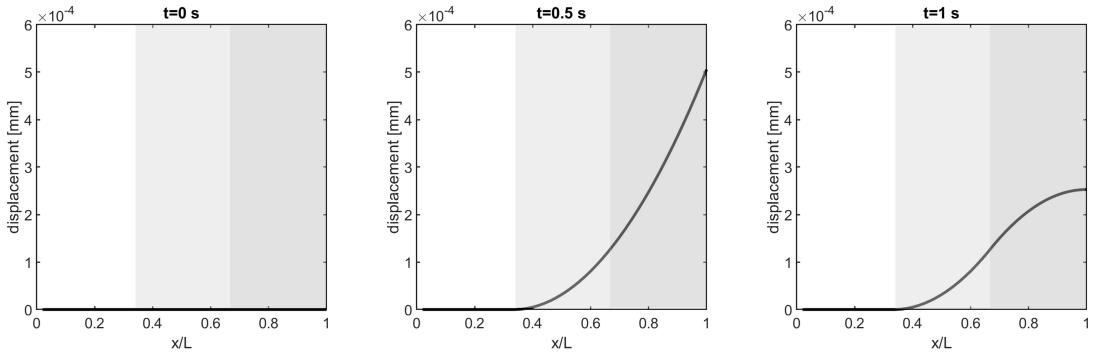

Figure 2: Displacement snapshots at time $t = 0$ s, $t = 0.5$ s and $t = 1$ s.

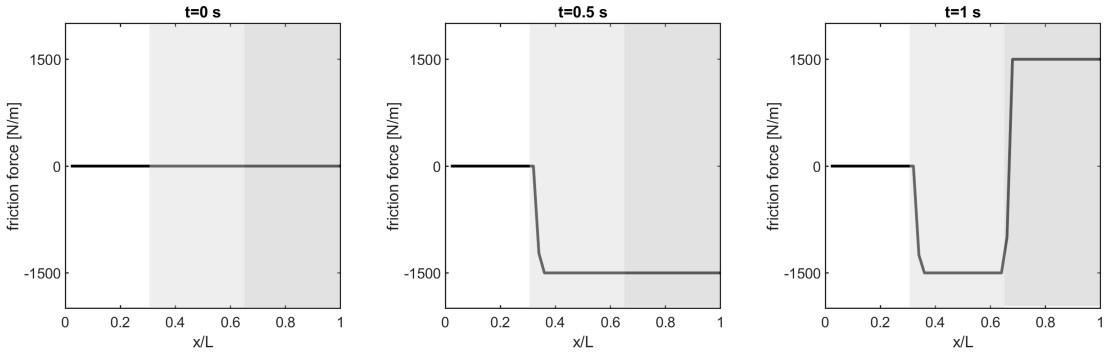

Figure 3: Frictional forces snapshots at time $t = 0$ s, $t = 0.5$ s and $t = 1$ s.

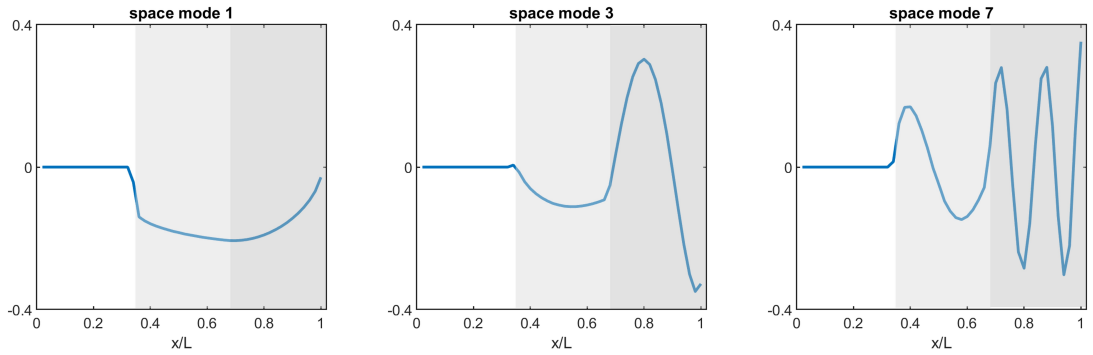

Figure 4: SVD space modes 1, 3 and 7 of the frictional contact forces.

In **Figure 5** is shown the SVD relative approximation error $\|\mathbb{A} - \mathbb{A}_p\|_F / \|\mathbb{A}\|_F$ between the original field and a truncated SVD of order p for displacements and frictional forces for the two considered loadcases in **Figure 1b**. The snapshot matrix $\mathbb{A}^{N_x \times N_t}$, which represents respectively the displacements or the frictional forces, collects the quantities of interest along the N_x spatial positions and N_t time steps, with $\mathbb{A}_p$ which represents the SVD approximation of $\mathbb{A}$ with p modes, and $\| \bullet \|_F$ stands for the Frobenius norm. In both cases, displacements present a better reducibility compared to frictional contact forces. Frictional contact forces, due to their highly non-smooth nature, present a very low reducibility, in agreement with similar results in [35, 37]. For the first loadcase (**Figure 5a**), the reducibility for frictional forces is quite critical. Being a propagation problem with a large sliding front, frictional forces need a large basis to reach a good accuracy (below 10^{-4}). For the second loadcase the reducibility of the problem strongly improves, especially for frictional forces, as in fact the small-amplitude oscillations cause small variations in contact

conditions, with a smaller size of the gray areas.

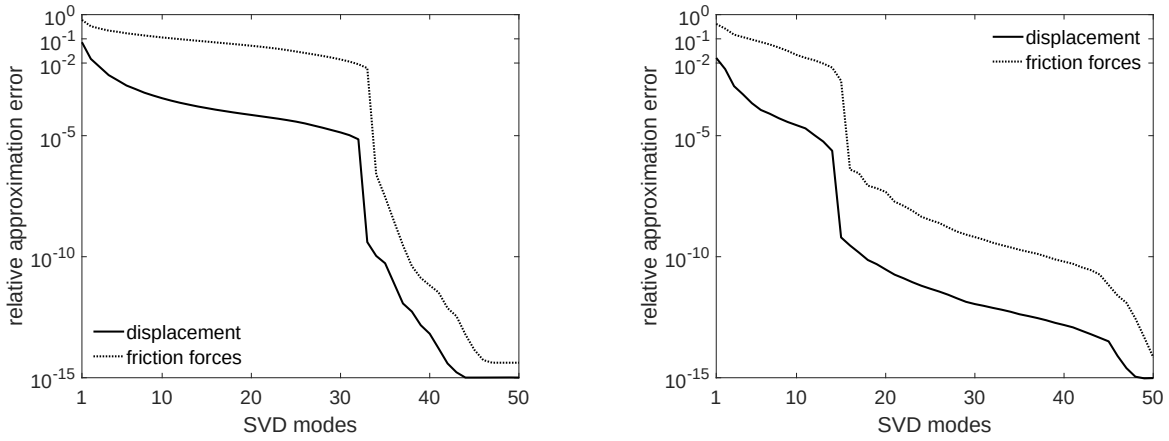

(a) SVD of loadcase 1.

(b) SVD of loadcase 2.

Figure 5: SVD of the contact quantites of the 1D problem in **Figure 1** for the two different loadcases.

Propagation problems are known for their low reducibility, and capturing their behavior with a ROB is challenging, even for ROBs enriched on-the-fly as in PGD [28, 47]. For particular applications where one deals with loads such like the second loadcase, or problems where the contact interface is small relatively to the overall structure of the problem, and/or a few contact interfaces are present, this can help to start with a good potential reducibility. However, in more complex and general cases like architectured materials [1], the peculiarities pertaining to contact problems can be taken into account to improve the efficiency of a model reduction approach. As seen in the above example, when wide contact interfaces are present, different areas subjected to different sticking and sliding conditions can be encountered. This suggests the separation of these different areas a priori and the application of the model reduction strategy separately, ideally in each part, through a DDM approach. Therefore, the different potential reducibility of the different areas is exploited and the computational time can further be improved thanks to the parallelization given by the DDM. Another aspect to consider is the presence of multiscale aspects in the solution of contact problems. As highlighted in [35], global modes on a structural level and localized modes on the contact interfaces are present and the introduction of multiscale aspects may effectively improve the handling of similar problems.

In the following, we will put ourselves in the case of the first loadcase, considered as more critical, and we will analyze how the proposed approach behaves in the case of a problem with low reducibility.

3. LATIN-based monoscale DDM for frictional contact problems

Incremental methods for solving a nonlinear problem (e.g., Newton-Raphson, quasi-Newton, modified Newton methods) consist in making converge the problem at a given time step t_j, knowing the converged solution from the previous time step t_{j-1}, up to the final time T. On the contrary, in non-incremental methods, all time steps are swept at each iteration and each non-incremental iteration ends on a space-time approximation of the solution. The LATIN method, introduced in [19], is a general strategy for dealing with nonlinear evolution problems and belongs to the family of non-incremental solvers.

The main idea of the LATIN is to separate the difficulties of a given problem. For many classes of problems this consists in avoiding the simultaneity of the global character of the problem and its local nonlinear behavior, which leads to a partitioning of the underlying equations into two manifolds: one pertaining to the local and possibly nonlinear equations, while the other one is related to the linear and possibly global equations. The search for the solution is based on a two search alternating direction algorithm, which shares similarities with ADMM (Alternating Direction Methods of Multipliers) methods [48, 49, 50]. At each iteration, a solution on the whole space and time

domain of the problem is alternately built in each of the two manifolds. A LATIN iterate being defined over the entire space-time domain, unlike an incremental method where only the solution at the previous step is generally required, inherently raises questions about the storage of computed quantities. The use of an adapted representation of the iterate in reduced or compact form, such as a representation in separate space and time variables [25], is therefore a necessity in terms of the method's efficiency. However, this constraint inherent to this particular nonlinear solver can also be seen as an advantage for model-order reduction by PGD as shown in the following.

When applied to contact problems, the LATIN method separates the internal equations belonging to the substructures from the contact conditions that occur at the contact interfaces. For this reason, it naturally leads to a mixed DDM where interface variables are constituted by the interface displacements (primal unknowns) and contact forces (dual unknowns). In addition, the two-search direction alternate algorithm of the LATIN shares similar features with augmented Lagrangian formulations combined with Uzawa-like algorithms [51, 52], which makes it a strongly robust strategy for dealing with contact problems, ensuring an exact satisfaction of contact conditions at convergence. Two types of formulations for the primal unknowns can be adopted: the formulation in velocity and the formulation in displacement. The velocity formulation is usually adopted in the context of material nonlinearities, where constitutive relations are expressed in a rate formulation (see [41, 53]), while the displacement formulation is usually more adopted in the context of linear elastic behaviour of the substructures [32, 35, 54], as in the case discussed herein.

3.1. The reference problem: partitioning into substructures and interfaces

We consider, assuming small perturbations and isothermal quasi-static state, the equilibrium of a linear elastic structure occupying the space domain Ω on the time interval $[0, T]$ being studied. The structure being subjected to body forces $\underline{f}_d$ and imposed loads $\underline{F}_d$ on a part $\partial_2\Omega$ of the boundary, as in **Figure 6**. On the complementary part $\partial_1\Omega$, displacements $\underline{U}_d$ are prescribed. Internal or external frictional contact interfaces are present and designated with Γ_c.

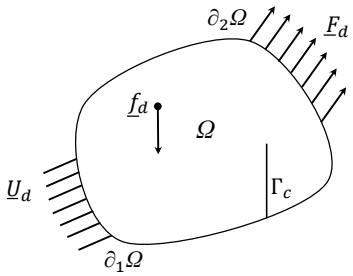

Figure 6: Reference structure problem being considered.

The basic idea of a mixed DDM strategy consists in describing the structure as an assembly of simple components: substructures and interfaces [19] (**Figure 7a**), where each substructure has its own variables and equations. A substructure Ω_E, with $E \in \mathbf{E}$ ($\mathbf{E}$ being the set of substructures), is subjected to the action of its environment $\mathbf{V}_E$ (i.e., the set of neighboring substructures of Ω_E) defined by a force field $\underline{F}_E$ and a displacement field $\underline{W}_E$ acting on its boundary $\partial\Omega_E$. The displacement and the Cauchy stress fields within a substructure Ω_E are denoted with $\underline{u}_E$ and $\boldsymbol{\sigma}_E$, and they belong respectively to spaces $\mathcal{U}_E^{[0,T]}$ and $\mathcal{S}_E^{[0,T]}$ defined on Ω_E. An interface $\Gamma_{EE'}$ between two substructures Ω_E and $\Omega_{E'}$ transfers both the displacement and the force fields $\underline{W}_E, \underline{W}_{E'}$ and $\underline{F}_E, \underline{F}_{E'}$ restricted to $\Gamma_{EE'}$ (**Figure 7b**), which belong respectively to spaces $\mathcal{W}_{EE'}^{[0,T]}$ and $\mathcal{F}_{EE'}^{[0,T]}$ defined on $\Gamma_{EE'}$. The previous spaces, extended to the set of neighboring interfaces of Ω_E, result in spaces $\mathcal{W}_E^{[0,T]}$ and $\mathcal{F}_E^{[0,T]}$. We denote with $\mathbf{E}_E^{[0,T]} = \mathcal{U}_E^{[0,T]} \times \mathcal{W}_E^{[0,T]}$ and $\mathbf{F}_E^{[0,T]} = \mathcal{S}_E^{[0,T]} \times \mathcal{F}_E^{[0,T]}$, as well as $\mathbf{S}_E^{[0,T]} = \mathbf{E}_E^{[0,T]} \times \mathbf{F}_E^{[0,T]}$. A space $\square^{[0,T]}$ with superscript $[0, T]$ designates the space of functions defined on $[0, T]$ which take values in $\square$. Therefore, one can define the admissibility of a solution within a substructure.

Definition 1 (E-admissibility)**.** For a substructure Ω_E, $\mathbf{s}_E = (\underline{u}_E, \underline{W}_E, \boldsymbol{\sigma}_E, \underline{F}_E) \in \mathbf{S}_E^{[0,T]}$ is said to be E-admissible, that is $\mathbf{s}_E \in \mathbf{S}_{E,\text{ad}}^{[0,T]}$, if it verifies:

– the kinematic admissibility: $(\underline{u}_E, \underline{W}_E) \in \mathbf{E}_{E,\text{ad}}^{[0,T]} \;\big|\; \exists\, \underline{u}_E \in \mathcal{U}_E^{[0,T]}$ such that $\underline{u}_E|_{\partial\Omega_E} = \underline{W}_E$,

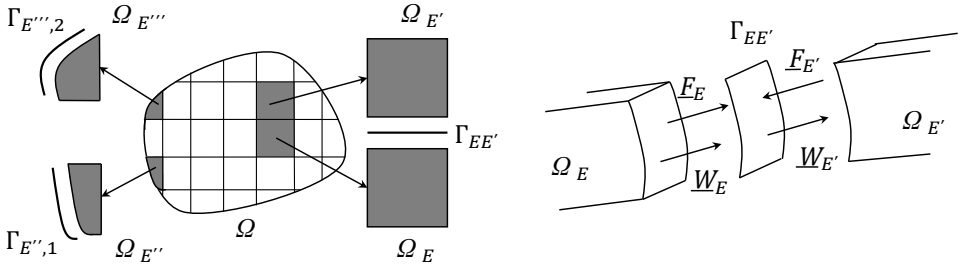

(a) Substructures and interfaces.

(b) Interface variables.

Figure 7: Decomposition of a structure.

– the static admissibility: $(\boldsymbol{\sigma}_E, \underline{F}_E) \in \mathbf{F}_{E,\text{ad}}^{[0,T]} \mid \forall (\underline{u}^*, \underline{W}^*) \in \mathbf{E}_{E,\text{ad}}^{[0,T]}$,

$$\int_{\Omega_E \times [0,T]} \boldsymbol{\sigma}_E : \boldsymbol{\varepsilon}(\underline{u}^*) \mathrm{d}\Omega \mathrm{d}t = \int_{\Omega_E \times [0,T]} \underline{f}_d \cdot \underline{u}^* \mathrm{d}\Omega \mathrm{d}t + \int_{\partial\Omega_E \times [0,T]} \underline{F}_E \cdot \underline{W}^* \mathrm{d}S \, \mathrm{d}t,$$

– the constitutive relation: $\boldsymbol{\sigma}_E = \boldsymbol{K} : \boldsymbol{\varepsilon}(\underline{u}_E)$, with $\boldsymbol{K}$ being the Hookean tensor and $\boldsymbol{\varepsilon}$ the small strain tensor.

An interface $\Gamma_{EE'}$ between two substructures Ω_E and $\Omega_{E'}$ is driven by a constitutive law between the force fields $(\underline{F}_E, \underline{F}_{E'})$ and the displacement fields $(\underline{W}_E, \underline{W}_{E'})$ on $\Gamma_{EE'}$. The constitutive behavior at the different interfaces depends on the type of interface behavior which is to be modeled, and is expressed as a constitutive law which can be formally written as:

$$\boldsymbol{b}_{EE'}(\underline{F}_E, \underline{W}_E, \underline{F}_{E'}, \underline{W}_{E'}) = \mathbf{0}, \ \forall (\underline{x}, t) \in \Gamma_{EE'} \times [0,T]. \tag{1}$$

The interface constitutive operator $\boldsymbol{b}_{EE'}$ describes in an abstract form the behavior of the interface. For example, for a perfect interface, $\boldsymbol{b}_{EE'} = \mathbf{0}$ corresponds to the continuity of the displacements across the interface, $\underline{W}_E - \underline{W}_{E'} = \underline{0}$, and the equilibrium of the interface forces $\underline{F}_E + \underline{F}_{E'} = \underline{0}$. Boundary conditions in displacements and forces are also taken into account through a specific interface behavior (interfaces $\Gamma_{E'',1}$ and $\Gamma_{E''',2}$ in **Figure 7a**). Then, the reference substructured problem can be reformulated as:

Problem 2. Find $\mathbf{s}_{\text{exact}} = \{\mathbf{s}_E\}_{E \in \mathbf{E}}$, with $\mathbf{s}_E = (\underline{u}_E, \underline{W}_E, \boldsymbol{\sigma}_E, \underline{F}_E) \in \mathbf{S}_E^{[0,T]}$, verifying:

– the E-admissibility of $\mathbf{s}_E$, $\forall E \in \mathbf{E}$: $\mathbf{s}_E \in \mathbf{S}_{E,\text{ad}}^{[0,T]}$ (**Definition 1**),

– the constitutive behavior of the interfaces (1) .

3.2. A LATIN-based iterative solver

Let us denote with $\mathbf{A}_d^{[0,T]}$ the manifold of linear elastic solutions $\mathbf{s}$ satisfying the E-admissibility, and refer with $\boldsymbol{\Gamma}^{[0,T]}$ to the manifold of solutions $\hat{\mathbf{s}}$ satisfying the constitutive behavior at the interfaces $\boldsymbol{b}_{EE'} = \mathbf{0}$. The LATIN method for solving **Problem 2** consists in iterating successively between manifolds $\mathbf{A}_d^{[0,T]}$, a phase which is called *linear stage*, and $\boldsymbol{\Gamma}^{[0,T]}$, named *local stage*, by following two alternating search direction equations $\mathbf{E}^+$ and $\mathbf{E}^-$ introduced to iterate in a fixed-point manner between the two manifolds and to close the problem. Starting from an initial admissible solution $\mathbf{s}_0$, at convergence the exact solution $\mathbf{s}_{\text{exact}}$ is reached at the intersection between the two manifolds:

$$\mathbf{s}_0 \in \mathbf{A}_d^{[0,T]} \Rightarrow \cdots \Rightarrow \mathbf{s}_n \in \mathbf{A}_d^{[0,T]} \xrightarrow[\mathbf{E}^+]{\text{local stage}} \hat{\mathbf{s}}_{n+1/2} \in \boldsymbol{\Gamma}^{[0,T]} \xrightarrow[\mathbf{E}^-]{\text{linear stage}} \mathbf{s}_{n+1} \in \mathbf{A}_d^{[0,T]} \Rightarrow \cdots \Rightarrow \mathbf{s}_{\text{exact}} \in \mathbf{A}_d^{[0,T]} \cap \boldsymbol{\Gamma}^{[0,T]}$$

3.2.1. The local stage

The local stage at the current iteration $n+1$ consists in finding $\hat{\mathbf{s}}_{n+1/2} \in \mathbf{\Gamma}^{[0,T]}$, given $\mathbf{s}_n \in \mathbf{A}_d^{[0,T]}$ from the previous iteration, by following the search direction $\mathbf{E}^+$. For each interface $\Gamma_{EE'}$ the following conditions must be verified, with the subscripts n and $n+1/2$ omitted to simplify the notations:

Problem 3 (*local stage*)**.** Find $\hat{\mathbf{s}} = \{\hat{\mathbf{s}}_E\}_{E\in\mathbf{E}} \in \mathbf{\Gamma}^{[0,T]}$ verifying, $\forall \underline{x} \in \Gamma_{EE'}$ and $\forall t \in [0,T]$,

$$\left\| \begin{array}{l} \text{– the interface constitutive behavior: } \boldsymbol{b}_{EE'}(\widehat{\underline{W}}_E, \widehat{\underline{W}}_{E'}, \widehat{\underline{F}}_E, \widehat{\underline{F}}_{E'}) = \mathbf{0} \\ \text{– the search direction } \mathbf{E}^+\text{: } \begin{cases} \widehat{\underline{F}}_E - \underline{F}_E - \boldsymbol{k}^+(\widehat{\underline{W}}_E - \underline{W}_E) = \underline{0} \\ \widehat{\underline{F}}_{E'} - \underline{F}_{E'} - \boldsymbol{k}^+(\widehat{\underline{W}}_{E'} - \underline{W}_{E'}) = \underline{0} \end{cases} \end{array} \right.$$

In the previous equations, $\boldsymbol{k}^+$ is called search direction operator (or simply search direction), usually taken as $\boldsymbol{k}^+ = k^+\mathbf{I}$, with $\mathbf{I}$ the identity tensor. The search direction parameter k^+ is homogeneous to a stiffness and analogous to the augmentation parameter in an augmented Lagrangian formulation. A reference close-to-optimal value for k^+, in the case of perfect interfaces, is given by $k^+ = E/L$, with E being the Young modulus of the substructure and L a characteristic length of the interface. The value of k^+ does not affect the result at convergence, although it has a significant impact on the convergence rate of the problem. The different interface behaviors and their explicit resolution on the local stage of the LATIN method are reported in Appendix A.

3.2.2. The linear stage

Given the solution $\hat{\mathbf{s}}_{n+1/2} \in \mathbf{\Gamma}^{[0,T]}$ from the local stage, the linear stage at the current iteration $n+1$ consists in finding $\mathbf{s}_{n+1} \in \mathbf{A}_d^{[0,T]}$ following a search direction $\mathbf{E}^-$:

Problem 4 (*linear stage*)**.** Find $\mathbf{s} = \{\mathbf{s}_E\}_{E\in\mathbf{E}} \in \mathbf{A}_d^{[0,T]}$ verifying, $\forall \underline{x} \in \Omega_E$ and $\forall t \in [0,T]$,

$$\left\| \begin{array}{l} \text{– the } E\text{-admissibility of } \mathbf{s}_E\text{: } \mathbf{s}_E \in \mathbf{S}_{E,\text{ad}} \\ \text{– the search direction } \mathbf{E}^- : \underline{F}_E - \widehat{\underline{F}}_E + \boldsymbol{k}^-(\underline{W}_E - \widehat{\underline{W}}_E) = \underline{0} \end{array} \right.$$

where it is classicaly assumed that $\boldsymbol{k}^- = \boldsymbol{k}^+ = \boldsymbol{k}$. Taking into account E-admissibility and the search direction, the following linear problem has to be solved at the linear stage for each substructure Ω_E in the whole space-time domain:

Problem 5. Find $(\underline{u}_E, \underline{W}_E) \in \mathbf{E}_{E,\text{ad}}^{[0,T]}$ such that, $\forall (\underline{u}^*, \underline{W}^*) \in \mathbf{E}_{E,\text{ad}}^{[0,T]}$,

$$\int_{\Omega_E\times[0,T]} \boldsymbol{\varepsilon}(\underline{u}_E) : \boldsymbol{K} : \boldsymbol{\varepsilon}(\underline{u}^*)\mathrm{d}\Omega\mathrm{d}t + \int_{\partial\Omega_E\times[0,T]} \boldsymbol{k}\underline{W}_E \cdot \underline{W}^*\mathrm{d}S\,\mathrm{d}t = \int_{\Omega_E\times[0,T]} \underline{f}_{d|\Omega_E} \cdot \underline{u}^*\mathrm{d}\Omega\mathrm{d}t + \int_{\partial\Omega_E\times[0,T]} (\widehat{\underline{F}}_E + \boldsymbol{k}\widehat{\underline{W}}_E) \cdot \underline{W}^*\mathrm{d}S\,\mathrm{d}t,$$

with $\underline{F}_E = \widehat{\underline{F}}_E + \boldsymbol{k}(\widehat{\underline{W}}_E - \underline{W}_E)$.

The solution of the linear stage problem associated with substructure Ω_E depends solely on the known quantities $\underline{f}_{d|\Omega_E}$ and $\hat{\mathbf{s}}_E$ on its boundary $\partial\Omega_E$. If $\boldsymbol{K}$ and $\boldsymbol{k}$ are symmetric positive definite, the **Problem 5** has a unique solution [19]. The linear stage problems defined on the different substructures Ω_E are independent and are therefore parallelizable.

3.2.3. Initialization and control of the convergence

The iterative LATIN algorithm is initialized with an admissible solution $\mathbf{s}_0 \in \mathbf{A}_d^{[0,T]}$. A classical choice is the solution obtained assuming $\hat{\mathbf{s}} = \mathbf{0}$, that is, for each substructure:

Problem 6 (*initialization*)**.** Find $(\underline{u}_{0,E}, \underline{W}_{0,E}) \in \mathbf{E}_{E,\text{ad}}^{[0,T]}$ such that, $\forall (\underline{u}^*, \underline{W}^*) \in \mathbf{E}_{E,\text{ad}}^{[0,T]}$,

$$\int_{\Omega_E\times[0,T]} \boldsymbol{\varepsilon}(\underline{u}_{0,E}) : \boldsymbol{K} : \boldsymbol{\varepsilon}(\underline{u}^*)\mathrm{d}\Omega\mathrm{d}t + \int_{\partial\Omega_E\times[0,T]} \boldsymbol{k}\underline{W}_{0,E} \cdot \underline{W}^*\mathrm{d}S\,\mathrm{d}t = \int_{\Omega_E\times[0,T]} \underline{f}_{d|\Omega_E} \cdot \underline{u}^*\mathrm{d}\Omega\mathrm{d}t,$$

with $\underline{F}_{0,E} = -\boldsymbol{k}\underline{W}_{0,E}$.

The monoscale strategy converges in presence of boundary condition interfaces, perfect interfaces and frictionless contact interfaces [19]. For contact interfaces with friction, there is no convergence proof of the algorithm but convergence is in practice obtained. To ensure the practical convergence of the method on a wider class of behaviors and interface types, a relaxation step is introduced after the linear stage:

$$\mathbf{s}_{n+1} \leftarrow \mu \mathbf{s}_{n+1} + (1-\mu)\mathbf{s}_n, \tag{2}$$

where $\mu \in [0,1]$ is the relaxation parameter, generally taken to be 0.8 [19].

In order to check the convergence of the LATIN algorithm, one can build LATIN convergence indicators based on the distance between two consecutive solutions belonging to each of the two manifolds. The classical convergence indicator adopted, introduced in [19], is the LATIN indicator:

$$\eta = \sqrt{\frac{\sum_E \|\mathbf{s}_E - \hat{\mathbf{s}}_E\|^2}{\frac{1}{2}\sum_E (\|\mathbf{s}_E\|^2 + \|\hat{\mathbf{s}}_E\|^2)}}, \text{ with } \|\mathbf{s}_E\|^2 = \int_{\partial\Omega_E \times [0,T]} (\boldsymbol{k} \underline{W}_E^2 + \boldsymbol{k}^{-1} \underline{F}_E^2) \mathrm{d}S\, \mathrm{d}t. \tag{3}$$

The LATIN indicator characterizes the global distance (i.e., in space and time) between the solution of the linear stage and the one belonging to the local stage for both displacements and interface forces, and is evaluated accounting for the whole set of interfaces. When the solution converges to $\mathbf{s}_{\text{exact}}$, the two consecutive iterates merge and the indicator tends to zero.

If the exact solution $\mathbf{s}_{\text{exact}}$ of the problem is available, one can compare the evolution of the LATIN indicator η with reference solutions errors in terms of interface displacements or interface forces, defined as follows:

$$\eta_W = \sqrt{\frac{\sum_E \|\underline{W}_E - \underline{W}_{E,\text{exact}}\|_2^2}{\sum_E \|\underline{W}_{E,\text{exact}}\|_2^2}} \text{ and } \eta_F = \sqrt{\frac{\sum_E \|\underline{F}_E - \underline{F}_{E,\text{exact}}\|_2^2}{\sum_E \|\underline{F}_{E,\text{exact}}\|_2^2}}, \text{ with } \|\square\|_2^2 = \int_{\partial\Omega_E \times [0,T]} \square^2 \mathrm{d}S\, \mathrm{d}t. \tag{4}$$

The LATIN indicator (Eq. (3)) gives an evaluation of the convergence of the problem in a global manner in space and time for all the possible domains and interfaces. It is clear that such a global convergence indicator does not guarantee that the solution has locally converged in space and time. For this reason, one could be also interested in looking for the error at a specific time value t by means of a LATIN time indicator η_t:

$$\eta_t = \sqrt{\frac{\sum_E \|\mathbf{s}_E(t) - \hat{\mathbf{s}}_E(t)\|_{\partial\Omega_E}^2}{\frac{1}{2}\sum_E (\|\mathbf{s}_E(t)\|_{\partial\Omega_E}^2 + \|\hat{\mathbf{s}}_E(t)\|_{\partial\Omega_E}^2)}}, \text{ with } \|\mathbf{s}_E(t)\|_{\partial\Omega_E}^2 = \int_{\partial\Omega_E} (\boldsymbol{k} \underline{W}_E^2(t) + \boldsymbol{k}^{-1} \underline{F}_E(t)^2) \mathrm{d}S. \tag{5}$$

A more severe convergence indicator has been proposed in [55], where a sup-norm over all the interfaces and all the space-time domain is considered. However, the previous error indicators are dependent on the search direction $\boldsymbol{k}$, and therefore, if $\boldsymbol{k}$ varies, for a given value of the error the solution may be significantly different. This point is crucial for contact problems where an accurate computation of local contact quantities is required, and it will be investigated in a future work.

3.3. Application on the 1D test problem

In this section, the monoscale LATIN method presented previously will be applied to the one-dimensional test problem described in **Section 2**, to highlight strengths of the method and critical points. The benchmark test of **Figure 1a** will be adopted, with the loadcase 1 of **Figure 1b** and the parameters of **Table 1**. We start with the case where only one substructure $\Omega_E = \Omega$, coincident with the space domain, is considered. A reference search direction parameter $k = k_0 = ES/L$ is chosen.

To emphasize the peculiarity of the LATIN to solve the nonlinear problem in a non-incremental manner, the solution obtained for the frictional contact forces, in space and time, along different iterations of the LATIN is shown in **Figure 8**. Already from the first iteration, the algorithm produces a global space-time view of the problem, which is subsequently refined locally along the iterations. **Figure 9a** shows the evolution of the LATIN indicator η (3) along the iterations, compared with the reference errors η_W and η_F (4). Displacements and interface forces have roughly the same convergence rate, although, for a fixed number of iterations, the interface forces are less accurate than the

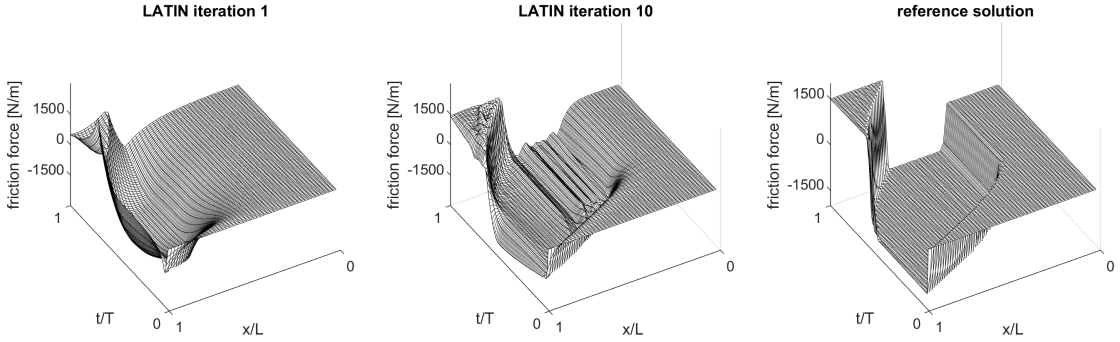

Figure 8: Space-time distribution of frictional forces along some LATIN iterations and reference solution.

displacements, and more critical to make converge. The LATIN indicator, which blends displacements and forces through the search direction $\boldsymbol{k}$, presents approximately the same rate of convergence as η_W and η_F, and an accuracy for a fixed number of iterations that lies in between the two. In **Figure 9b** is shown the LATIN time indicator η_t (5) along the time interval at different iterations. As expected, the error on the different time steps is not uniform.

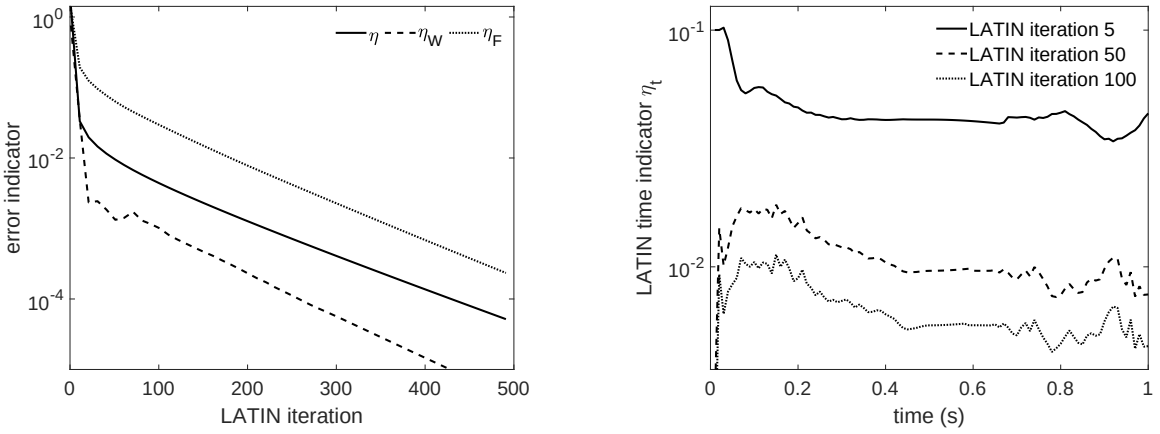

(a) LATIN indicator η and error indicators η_W and η_F.

(b) LATIN time indicator η_t.

Figure 9: LATIN convergence and error indicators.

As mentioned previously, the value of the parameter k that one makes use of in the LATIN algorithm affects the convergence rate of the problem, but not the result at convergence, which renders the method strongly robust for whatever complex loading and any number of frictional contact interfaces. The results in **Figure 10a** show how different values of k affect the convergence rate of the algorithm. The optimal search direction parameter k for frictional contact problems, which guarantees the best convergence rate, is not known a priori since it depends on the particular problem. It is crucial also to evaluate the influence of the search direction parameter k on the quality of a converged solution. In **Figure 10b** is shown a snapshot of the frictional forces distribution at time $t = 0.5$ s of the problem solved with three different values of the search direction parameter, $k = k_0 = ES/L$, $k = 0.1\ k_0$ and $k = 10\ k_0$, until reaching a LATIN convergence indicator threshold of $\eta = 10^{-3}$. A good convergence indicator should provide solutions of comparable quality whatever the value of the search direction adopted, for a fixed value of the convergence threshold. In this case one can notice that for a given convergence threshold η, the solutions provided for different values of the search directions are quite different. In particular, the error concerns mostly the accurate identification of the sticking-sliding transition zones. The issue of proposing a convergence indicator independent

from $\boldsymbol{k}$ will be addressed in a later article.

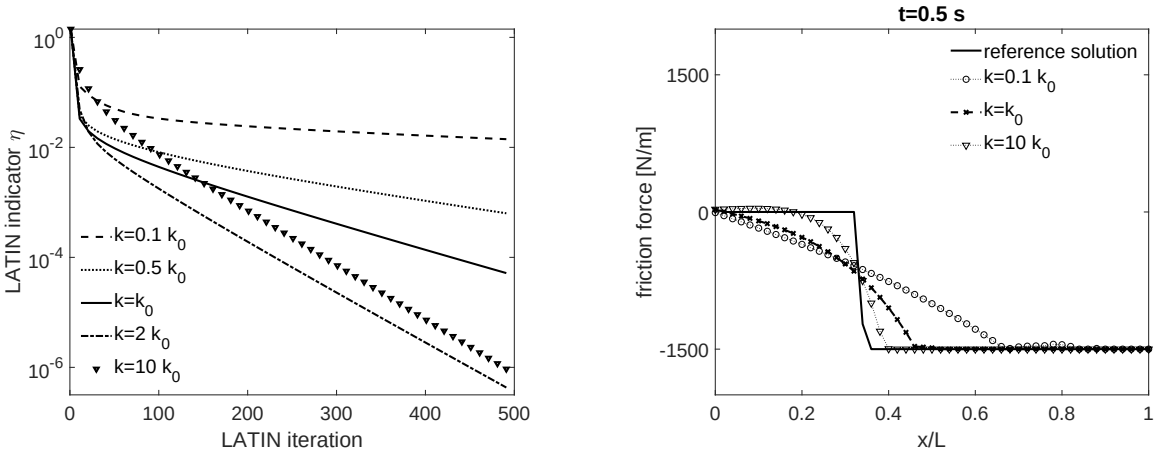

(a) Influence of the search direction parameter k on the convergence rate of the LATIN method.

(b) Influence of the search direction parameter k on the solution quality for a given value of $\eta = 10^{-3}$.

Figure 10: Influence of the search direction parameter k.

A monostructure case of the problem was considered in previous results. The LATIN, however, naturally leads to a monoscale domain decomposition method. Let us consider how the solution of the original problem behaves by partitioning it into substructures, as in **Figure 11**. Each substructure is assigned the parameters of **Table 1**, and each substructure is linked to the neigbouring ones through perfect interfaces.

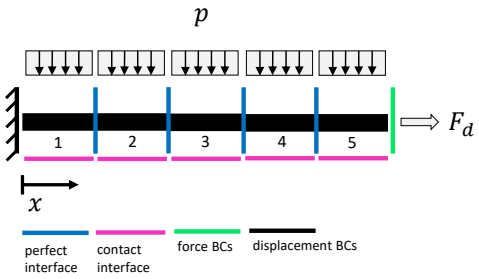

Figure 11: Substructured 1D test problem into 5 substructures, with respective numbering.

Figure 12a shows, in the case of 10 substructures, the frictional forces distribution at time $t = 0.5$ s along some iterations of the LATIN. The monoscale nature of the approach allows the exchange of information only between neighboring substructures. In the first iteration, only the substructure directly subject to the external load sees the effect of the loading. The influence of the external load is then slowly propagated to the remaining substructures iteration after iteration, which causes a decrease of the convergence rate with the number of substructures (**Figure 12b**). This domain decomposition strategy is clearly not numerically scalable. It will be shown subsequently in **Section 5** how the multiscale strategy allows to address this issue as well.

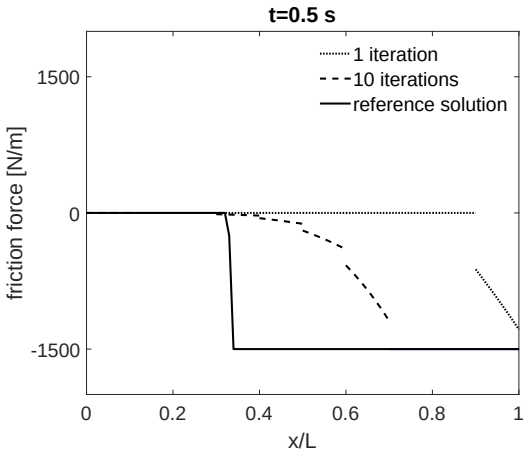

(a) Frictional forces solution at time $t = 0.5$ s with 10 substructures with the monoscale LATIN-DDM.

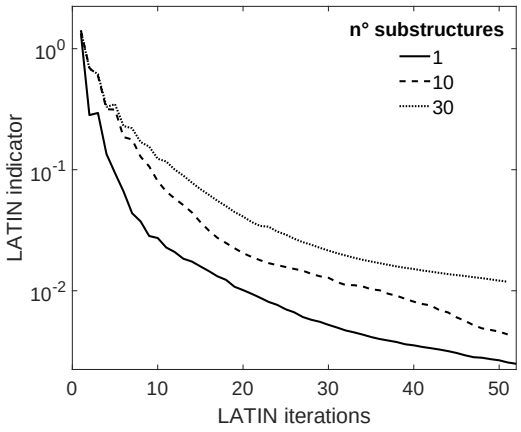

(b) Influence of the number of substructures on the convergence of the monoscale LATIN-DDM.

Figure 12: Monoscale LATIN-DDM applied to the substructured 1D problem in **Figure 11**.

4. Solving linear stage problems with PGD

The linear stage of the LATIN algorithm, as described in **Section 3**, consists in solving independently, for each substructure Ω_E, a linear problem on the whole space-time domain. For this reason, it is suitable for model-order reduction based on the separation of variables. In particular, a priori model reduction based on the PGD [28] can be introduced in the linear stage of the LATIN method in order to speed up the computations [19, 39, 56].

First of all, starting from the initial linear elastic solution $\mathbf{s}_0$ given by **Problem 6**, let us write the solution $\mathbf{s}_{n+1}$ at the current iteration as a correction with respect to the previous iteration solution, that is $\mathbf{s}_{n+1} = \mathbf{s}_n + \Delta\mathbf{s}$. Given the linearity of the equations pertaining to the manifold $\mathbf{A}_d^{[0,T]}$, the E-admissibility conditions and the search direction equation can be equivalently written, for each substructure Ω_E, in terms of corrections.

Definition 7 (E-admissibility to zero)**.** $\Delta\mathbf{s}_E = (\Delta\underline{u}_E, \Delta\underline{W}_E, \Delta\boldsymbol{\sigma}_E, \Delta\underline{F}_E) \in \mathbf{S}_E^{[0,T]}$ is said to be E-admissible to zero, that is $\Delta\mathbf{s}_E \in \mathbf{S}_{E,\mathrm{ad},0}^{[0,T]}$, if it verifies:

- the kinematic admissibility to zero: $(\Delta\underline{u}_E, \Delta\underline{W}_E) \in \mathbf{E}_{E,\mathrm{ad},0}^{[0,T]} \;\big|\; \exists\, \Delta\underline{u}_E \in \mathcal{U}_E^{[0,T]}$ such that $\Delta\underline{u}_E|_{\partial\Omega_E} = \Delta\underline{W}_E$,
- the static admissibility to zero: $(\Delta\boldsymbol{\sigma}_E, \Delta\underline{F}_E) \in \mathbf{F}_{E,\mathrm{ad},0}^{[0,T]} \;\big|\; \forall(\underline{u}^*, \underline{W}^*) \in \mathbf{E}_{E,\mathrm{ad},0}^{[0,T]}$,

$$\int_{\Omega_E\times[0,T]} \Delta\boldsymbol{\sigma}_E : \boldsymbol{\varepsilon}(\underline{u}^*)\mathrm{d}\Omega\mathrm{d}t = \int_{\partial\Omega_E\times[0,T]} \Delta\underline{F}_E \cdot \underline{W}^*\mathrm{d}S\,\mathrm{d}t,$$

- the constitutive relation: $\Delta\boldsymbol{\sigma}_E = \boldsymbol{K} : \boldsymbol{\varepsilon}(\Delta\underline{u}_E)$.

Similarly, the search direction equation $\mathbf{E}^-$ at the current iteration $n+1$ can be equivalently written as

$$\Delta\underline{F}_E + \boldsymbol{k}\Delta\underline{W}_E - \underline{\delta}_E = \underline{0}, \tag{6}$$

with the quantity $\underline{\delta}_E = \widehat{\underline{F}}_E + \boldsymbol{k}\widehat{\underline{W}}_E - (\underline{F}_{E,n} + \boldsymbol{k}\underline{W}_{E,n})$ known at the current iteration, and which depends on the previous local and linear stage. By taking into account kinematic and static admissibility to zero and the constitutive relation, the equivalent problem in terms of corrections to be solved at the linear stage is the following linear problem:

Problem 8. Find $(\Delta\underline{u}_E, \Delta\underline{W}_E) \in \mathbf{E}^{[0,T]}_{E,\mathrm{ad},0}$ such that, $\forall (\underline{u}^*, \underline{W}^*) \in \mathbf{E}^{[0,T]}_{E,\mathrm{ad},0}$,

$$\int_{\Omega_E\times[0,T]} \boldsymbol{\varepsilon}(\Delta\underline{u}_E) : \boldsymbol{K} : \boldsymbol{\varepsilon}(\underline{u}^*)\mathrm{d}\Omega\mathrm{d}t = \int_{\partial\Omega_E\times[0,T]} \Delta\underline{F}_E \cdot \underline{W}^*\mathrm{d}S\,\mathrm{d}t,$$

with $\Delta\underline{F}_E + \boldsymbol{k}\Delta\underline{W}_E - \underline{\delta}_E = \underline{0}$.

A progressive construction of space-time functions for PGD is classicaly used [28], and consists in looking for a separated representation solution of **Problem 8** for the corrections of forces and displacements, that is

$$\Delta\underline{u}_E = \underline{z}(\underline{x})\lambda(t) \text{ on } \Omega_E\times[0,T],\ \Delta\underline{W}_E = \underline{Z}(\underline{x})\lambda(t) \text{ and } \Delta\underline{F}_E = \underline{G}(\underline{x})\psi(t) \text{ on } \partial\Omega_E\times[0,T], \tag{7}$$

where $\lambda, \psi \in \mathcal{J} = \mathcal{L}^2_{[0,T]}$ and time functions of $\Delta\underline{u}_E$ and $\Delta\underline{W}_E$ are taken equal for kinematic admissibility. By injecting the separated representations (7) in **Problem 8**, and by making use of trial functions $\underline{u}^* = \underline{z}^*\lambda + \underline{z}\lambda^*$ and $\underline{W}^* = \underline{Z}^*\lambda + \underline{Z}\lambda^*$ belonging to $\mathbf{E}^{[0,T]}_{E,\mathrm{ad},0}$, one obtains the following two conditions to be satisfied in order for the separated representations (7) to be admissible:

$$\forall\lambda^* \in \mathcal{J},\ \int_{[0,T]} \lambda\lambda^* dt \int_{\Omega_E} \boldsymbol{\varepsilon}(\underline{z}) : \boldsymbol{K} : \boldsymbol{\varepsilon}(\underline{z})\mathrm{d}\Omega = \int_{[0,T]} \psi\lambda^*\mathrm{d}t \int_{\partial\Omega_E} \underline{G}\cdot\underline{Z}\mathrm{d}S, \tag{8}$$

$$\forall(\underline{z}^*, \underline{Z}^*) \in \mathbf{E}_{E,\mathrm{ad},0},\ \int_{\Omega_E} \boldsymbol{\varepsilon}(\underline{z}) : \boldsymbol{K} : \boldsymbol{\varepsilon}(\underline{z}^*)\mathrm{d}\Omega \int_{[0,T]} \lambda^2\mathrm{d}t = \int_{\partial\Omega_E} \underline{G}\cdot\underline{Z}^*\mathrm{d}S \int_{[0,T]} \lambda\psi\mathrm{d}t. \tag{9}$$

In Eq. (9), the space $\mathbf{E}_{E,\mathrm{ad},0}$ is the space of kinematic admissibility to zero for functions not depending on time, such as space modes $\underline{z}$, $\underline{Z}$ and $\underline{G}$. Similarly, in the following, $\mathbf{S}_{E,\mathrm{ad},0}$ will indicate the E-admissibility to zero for space modes (see **Definition 7**). From Eq. (8), the arbitrary of λ^* enables one to say that, up to a multiplicative constant, $\psi(t) = \lambda(t)$, $\forall t \in [0,T]$. On the other hand, from Eq. (9), the following admissibility condition between space modes of forces and displacements holds:

$$\forall(\underline{z}^*, \underline{Z}^*) \in \mathbf{E}_{E,\mathrm{ad},0},\ \int_{\Omega_E} \boldsymbol{\varepsilon}(\underline{z}) : \boldsymbol{K} : \boldsymbol{\varepsilon}(\underline{z}^*)\mathrm{d}\Omega = \int_{\partial\Omega_E} \underline{G}\cdot\underline{Z}^*\mathrm{d}S. \tag{10}$$

These two conditions (i.e., time modes being equal and space modes verifying condition (10)) have to be satisfied by the space and time modes of the separated representation of the current linear stage to belong to the admissible space $\mathbf{A}^{[0,T]}_d$ of the LATIN algorithm. However, with such an admissible separated representation, the search direction equation (6), rewritten as $(\underline{G} + \boldsymbol{k}\underline{Z})\lambda - \underline{\delta}_E = \underline{0}$, cannot be strictly verified since $\underline{\delta}_E$ is not in a separated format.

4.1. Finding a new pair of modes

The admissibility condition of Eq. (10) guarantees that the separated representation lies in the admissible space $\mathbf{A}^{[0,T]}_d$. However, the search direction can be verified only in a weak sense:

Problem 9 (*enrichment stage*)**.** Find $(\underline{z}, \underline{Z}, \underline{G}) \in \mathbf{S}_{E,\mathrm{ad},0}$ and $\lambda \in \mathcal{J}$ minimizing the error in search direction

$$(\underline{Z}, \underline{G}, \lambda) = \arg \min_{(\overline{\underline{G}}, \overline{\underline{Z}}, \overline{\lambda}) \in \mathbf{S}_{E,\mathrm{ad},0}\times\mathcal{J}} \|(\overline{\underline{G}} + \boldsymbol{k}\overline{\underline{Z}})\overline{\lambda} - \underline{\delta}_E\|^2_2, \tag{11}$$

and satisfying the admissibility condition of Eq. (10), with $\|\square\|^2_2 = \displaystyle\int_{\partial\Omega_E\times[0,T]} \square^2\mathrm{d}S\,\mathrm{d}t$.

In order to solve the above defined problem, an auxiliary mixed space mode, defined on the boundary $\partial\Omega_E$, is introduced [35]:

$$\underline{L} := \underline{G} + \boldsymbol{k}\underline{Z}. \tag{12}$$

Subsequently, the minimization problem of Eq. (11) is solved for $\underline{L}$ and λ with a fixed point iterative strategy, shown in **Algorithm 1**, where we arbitrarily choose to normalize space modes. The first step consists in computing $\underline{L}$ knowing λ from the previous iteration. Then, the second step consists in updating λ knowing $\underline{L}$ from the first step. After few

iterations (two or three are usually enough), $\underline{L}$ and λ are no more significantly updated and the process is stopped [28]. Then, by making use of admissibility condition (10), one can retrieve the admissible $\underline{z}$, $\underline{Z}$ and $\underline{G}$ space modes from $\underline{L}$. Therefore, $\underline{\delta}_E$ is approximated as $\underline{\delta}_E = \widehat{\underline{F}}_E + \boldsymbol{k}\widehat{\underline{W}}_E - (\underline{F}_{0,E} + \boldsymbol{k}\underline{W}_{0,E} + \sum_{k=1}^{p+1} \underline{L}_k\lambda_k)$, and solution fields, which

Algorithm 1: Enrichment stage: new pair of PGD modes

■ initialization: $\lambda(t) = 1$
for $n = 1$ to $n_{\max}$ **do**
– compute space mode: $\underline{L} = \int_{[0,T]} \underline{\delta}_E\lambda \,\mathrm{d}t \Big/ \int_{[0,T]} \lambda^2 \,\mathrm{d}t$
– compute time mode: $\lambda = \int_{\partial\Omega_E} \underline{\delta}_E \cdot \underline{L} \,\mathrm{d}S \Big/ \int_{\partial\Omega_E} \underline{L}^2 \,\mathrm{d}S$
– normalize space mode: $\underline{L} \leftarrow \underline{L}/\|\underline{L}\|$
– amplify time mode: $\lambda \leftarrow \lambda\|\underline{L}\|$

are admissible, can be written in a separated representation as $\underline{u}_E = \underline{u}_{0,E} + \sum_{k=1}^{p+1} \underline{z}_k\lambda_k$, $\underline{W}_E = \underline{W}_{0,E} + \sum_{k=1}^{p+1} \underline{Z}_k\lambda_k$ and $\underline{F}_E = \underline{F}_{0,E} + \sum_{k=1}^{p+1} \underline{G}_k\lambda_k$, with $p+1$ being the current PGD basis size after the enrichment stage.

The minimization problem (11), since the substructure is linear and search directions only concern interface quantities, is defined in space on the substructure boundary. When generating new modes the most costly part concerns the generation of space modes, due to the admissibility condition (10), which requires the resolution of a problem in space of the size of the substructure. For this reason, prior to adding a new pair of modes in the enrichment stage, if a given basis of p modes $\{\underline{L}_k, \lambda_k\}_{k=1}^p$ is available, a preliminary updating of time modes can be performed by keeping fixed the space modes, as shown in **Problem 10**. The updating stage consists in a cheap projection onto the current PGD basis and, since space modes are fixed (i.e., they are already admissible), there is no need to verify admissibility condition for the p space modes.

Problem 10 (*preliminary updating stage*)**.** Find $\Delta\lambda_k \in \mathcal{T}$, $k = 1, \ldots, p$ minimizing the error in search direction

$$\{\Delta\lambda_k\}_{k=1}^p = \arg\min_{\Delta\overline{\lambda}_k \in \mathcal{T}} \| \textstyle\sum_{k=1}^p \underline{L}_k\Delta\overline{\lambda}_k - \underline{\delta}_E\|_2^2, \tag{13}$$

and subsequently update time modes $\{\lambda_k\}_{k=1}^p \leftarrow \{\lambda_k\}_{k=1}^p + \{\Delta\lambda_k\}_{k=1}^p$.

The updating stage largely improves the quality of the PGD representation [28]. After the updating stage, if the quality of the representation is not satisfactory, one proceeds to add a new pair (or more) of modes. This step is crucial. In fact, for a better efficiency of the method, it is necessary to create the minimum amount of modes and to avoid the creation of redundant and unnecessary ones, as shown in the next **Section 4.2**.

Remark 11. Since nonlinearities are confined only to interfaces, search directions have been introduced only for interface quantities, resulting into a simple interface residual minimization for the generation of a new mode. For more general nonlinear problems where nonlinearities can also occur within the substructures, search directions have to be introduced for quantities defined on both interfaces and substructures, resulting into a more involved formulation. For material nonlinearities, interested readers can refer to [41, 53, 57].

4.2. Controlling the size and quality of the PGD basis

A generally adopted enrichment criterion (e.g., in [35]) used to decide whether to add or not a new pair of modes is the one based on the LATIN indicator stagnation. Given the LATIN indicator η at the previous iteration, and $\widetilde{\eta}$ after the updating stage (**Problem 10**), a new pair of modes is added if the following stagnation criterion is satisfied:

$$\theta = \frac{\eta - \widetilde{\eta}}{\eta} < \theta_0. \tag{14}$$

However, this indicator is poorly suited for frictional contact problems. In fact, as shown in **Figure 10a**, the convergence rate of the LATIN is mainly dependent on the search direction parameter k. Since in the presented formulation admissibility is exactly verified and only the search direction is approximated (see **Problem 9**), after a certain point

adding new modes will not improve the convergence rate, which is driven by k, and new useless modes would be consistently added. A more appropriate criterion is naturally based on the definition of the separated representation itself, according to **Problem 9**. In fact, what one approximates is the quantity $\underline{\delta}_E$ at every iteration (see Eq. (11)). For this reason, it is natural to choose a criterion based on the accuracy of the approximated search direction:

$$\xi = \frac{\|\underline{\delta}_E - \widetilde{\underline{\delta}}_E\|_2}{\|\underline{\delta}_E\|_2} > \xi_0, \tag{15}$$

where $\widetilde{\underline{\delta}}_E = \widehat{\underline{F}}_E + \boldsymbol{k}\widehat{\underline{W}}_E - (\underline{F}_{0,E} + \boldsymbol{k}\underline{W}_{0,E} + \sum_{k=1}^{p} \underline{L}_k(\lambda_k + \Delta\lambda_k)$ is the approximation of the search direction after the updating stage, by keeping constant the space basis $\{\underline{L}_k\}_{k=1}^{p}$. In both cases, a threshold of 0.1 is commonly adopted. In the θ-criterion (14), this corresponds to a decrease of the LATIN indicator by a factor less than 10%, while, in the ξ-criterion (15), it corresponds to an approximation of the search direction with a relative error more than 10%.

A reasonable enrichment criterion is crucial for the PGD basis not to grow uncontrollably in size, loosing effectiveness of the method. For highly non-regular phenomena like frictional contact problems, it is challenging to create progressively a ROB of the smallest size possible to ensure a given accuracy, that is to be close to the SVD basis of the final solution. The progressively found PGD modes may be highly redundant even when performing the updating stage, and the basis size may increase with modes which add little to no contribution to the representation accuracy. This problem can be palliated, for example, by systematically performing a Gram–Schmidt orthonormalization for the space modes. However, even after orthonormalization of space modes, redundancy may still occur on time modes [58]. An approach that can be adopted is to perform a full SVD computation of the solution after each enrichment step, and to keep the most significant modes as basis for the next iteration. Less expensive methods could make use of SVD updating techniques [59, 60] or randomized SVD [58]. However, these methods aim at computing precisely the SVD of the solution throughout the iterations of the LATIN, with an effort which may be not worthwhile knowing that the solution may be far from convergence. In [35], in the context of frictional contact problems, an iterative sorting and downsizing algorithm has been proposed to decrease the size of the PGD basis throughout the LATIN iterations, while maintaining a given quality of the solution. At convergence, the algorithm is equivalent to an SVD, however, since it is not required to compute exactly the SVD at each LATIN iteration, few iterations (1 or 2) of the algorithm at each LATIN iteration are sufficient for the purpose. Applied in the case of the monoscale LATIN method without domain decomposition, the downsizing algorithm is indeed effective in controlling the size and quality of the reduced basis. However, it will be shown throughout this paper (**Section 6**) that it may still be too costly and that, with a proper choice of the enrichment criterion and taking into account the multiscale aspects of contact problems through a multiscale approach based on DDM, it is possible to create PGD reduced bases of controlled size and good quality without resorting to SVD-like techniques.

4.3. Application on the 1D test problem

Here, the LATIN-PGD strategy is applied to the resolution of the benchmark problem illustrated **Figure 1a**, with the loadcase 1 of **Figure 1b** and the parameters of **Table 1**. The monostructure case $\Omega_E = \Omega$ without DDM is considered. The goal is to study deeply the PGD only.

First, the LATIN-PGD algorithm with the θ enrichment criterion (14), with $\theta_0 = 0.1$, is considered. A first strategy consists in adding a new pair of modes any time the enrichment criterion (14) is satisfied after the updating stage (LATIN-PGD(θ)), without making use of sorting algorithms for the PGD basis. A second strategy consists in performing also a Gram–Schmidt orthonormalization of the space modes any time a new pair of modes is added (LATIN-PGD(θ)+GS), and a third one consists in performing an additional downsizing stage (see Appendix B) for the PGD basis at each LATIN iteration (LATIN-PGD(θ)+D). In the LATIN-PGD(θ)+D strategy, a single iteration of the downsizing algorithm presented in [35] is performed at each LATIN iteration, and a threshold $\epsilon = 10^{-4}$ is chosen for the mode rejection. The different strategies investigated throughout the paper and their properties are reported in **Table 2**. We consider to add at most one pair of modes after the updating stage. In fact, more pairs of modes can be added at each LATIN iteration, however, adding more modes leads to increase the PGD basis with unnecessary modes when far from convergence.

Figure 13b shows the evolution of the PGD basis size along the LATIN iterations by making use of the three different strategies described previously. Regarding the LATIN-PGD(θ), the basis size largerly exceeds the original

LATIN-PGD strategies			
Strategy	ROB enrichment criterion	ROB sorting algorithm	Comments
full LATIN	-	-	no PGD
LATIN-PGD(θ)	θ-criterion (14)	-	no ROB sorting algorithm
LATIN-PGD(θ)+GS	θ-criterion (14)	Gram–Schmidt	only space modes are sorted
LATIN-PGD(θ)+D	θ-criterion (14)	downsizing (Appendix B)	low-cost SVD algorithm [35]
LATIN-PGD(ξ)	ξ-criterion (15)	-	no ROB sorting algorithm
LATIN-PGD(ξ)+D	ξ-criterion (15)	downsizing (Appendix B)	low-cost SVD algorithm [35]

Table 2: Different LATIN-PGD strategies investigated throughout the paper.

size of the problem (considering the problem size in space variable, a maximum of 50 modes is required for an exact evaluation of the quantities, see **Figure 5a**). Given the particular behavior of the LATIN convergence indicator, with a high rate in the first iterations (almost independent from the search direction parameter k) and a lower rate in the subsequent iterations (controlled by the value of k), the θ-criterion generates less modes in the first part and more modes in the second one. However, since the convergence rate in this second part is driven by the search direction parameter k, most of the generated modes will be useless.

The curve in **Figure 13b** of the LATIN-PGD(θ)+D confirms the previous hypothesis on the useless modes generated. In fact, the downsizing algorithm does not reduce the size of the basis in the first part of the LATIN iterations, while, after a certain point (approximately after iteration 40, where the LATIN indicator curve changes slope), most of the newly added modes are rejected. The final size of the downsized basis lays between 30 and 40 modes, which is the size required for the contact quantites to be accurately represented (see **Figure 5a**). Finally, the LATIN-PGD(θ)+GS shows to be uneffective to control the basis size, as it just limits the basis size not to exceed the size of the problem.

Figure 13a shows the behaviour of the LATIN indicator for the full LATIN (i.e., without PGD) and the different LATIN-PGD(θ) strategies. The high slope initial convergence is oscillating and not well captured, while the second part of the curve, where a new mode is generated almost systematically, is more uniform and tends to the full LATIN curve. The convergence curves of the different LATIN-PGD(θ) strategies described are in practice coincident, since the goal of ROB sorting methods is to control the size of the progressively built PGD basis without losing appreciable accuracy.

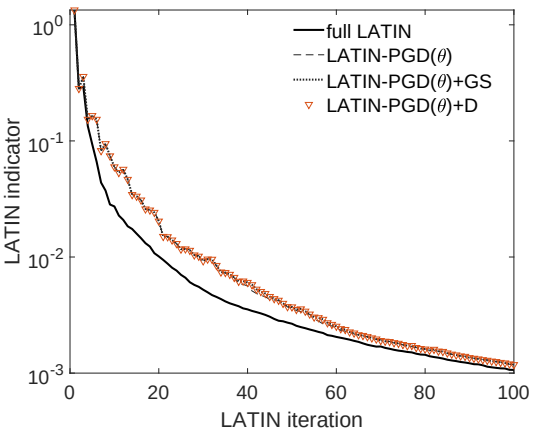

(a) LATIN convergence indicator for full LATIN, LATIN-PGD(θ), LATIN-PGD(θ)+GS and LATIN-PGD(θ)+D.

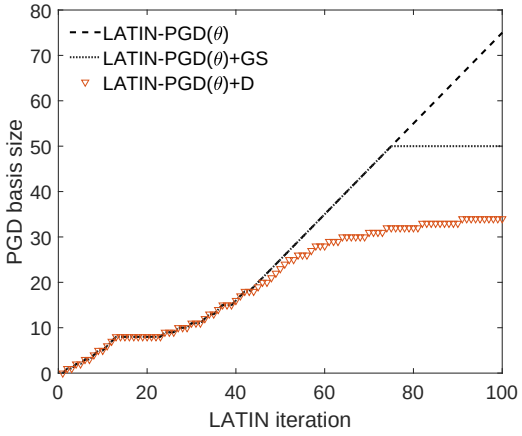

(b) Basis size along the LATIN iterations of the LATIN-PGD(θ), LATIN-PGD(θ)+GS and LATIN-PGD(θ)+D.

Figure 13: Convergence curves and PGD basis analysis for the LATIN-PGD(θ) strategies.

The behavior of the PGD basis along the iterations with the LATIN-PGD(θ)+D can be easily visualized by making use of the Modal Assurance Criterion (MAC) diagrams between the PGD modes and the SVD modes [61]. Shortly, given two sets of vectors of the same dimension $\{\mathbf{X}_i\}_{i=1}^{p}$ and $\{\mathbf{Y}_j\}_{j=1}^{p}$, the MAC matrix $\mathbf{M}$ is defined as:

$$\mathbf{M}_{ij} = \frac{|\mathbf{X}_i^T \mathbf{Y}_j|^2}{\|\mathbf{X}_i\|^2 \|\mathbf{Y}_j\|^2} \in [0, 1]. \tag{16}$$

$\mathbf{M}_{ij}$ measures the correlation between mode $\mathbf{X}_i$ and mode $\mathbf{Y}_j$. $\mathbf{M}_{ij} = 1$ means that the modes are collinear, that is highly correlated, otherwise $\mathbf{M}_{ij} = 0$ means that the modes are orthogonal, that is highly uncorrelated. At every LATIN iteration n, a full SVD of the linear stage solution $\underline{F}_n + \boldsymbol{k}\underline{W}_n$ for the mixed quantity is computed and compared to downsized PGD modes $\{\underline{L}_k\}$ (12) by making use of the MAC criterion definition (16).

Figure 14 displays the MAC diagram for the auxiliary mixed modes. The downsizing algorithm provides along the iterations a quasi-optimal basis correlated to the SVD (as shown in [35]). The resultant correlation for downsized space modes $\{\underline{Z}_k\}$ and $\{\underline{G}_k\}$, not shown here, obtained from the admissibility condition of Eq. (10), is still good but not as accurate as for $\{\underline{L}_k\}$.

Nevertheless, the PGD strategy is based on the approximation of the search direction through space modes $\{\underline{L}_k\}$, from which the admissible space modes $\{\underline{Z}_k\}$ and $\{\underline{G}_k\}$ are obtained through the solution of a problem in space at the substructure level. Although applying downsizing to the $\{\underline{L}_k\}$ basis is cheap, after the process, to compute the downsized space basis $\{\underline{Z}_k\}$ and $\{\underline{G}_k\}$ of displacements and frictional forces, equation (10) must be solved again for all the basis and this step may be expensive, as it will be shown on a more complicated 2D case in **Section 6**. It is therefore clear that the most important thing is to choose a relevant enrichment criterion, and a proper strategy, which enable to generate relevant modes and reduce the generation of redundant and useless ones.

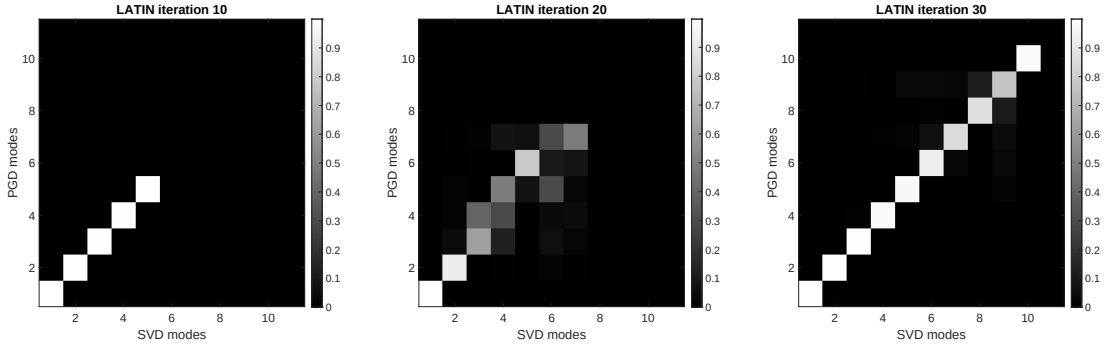

Figure 14: MAC diagrams for auxiliary space modes $\{\underline{L}_k\}$ along the iterations of the LATIN method.

Let us consider now the LATIN-PGD(ξ) strategy by making use of the ξ criterion (15), with $\xi_0 = 0.1$, without resorting to orthonormalization or downsizing. **Figure 15a** shows the LATIN-PGD(ξ) strategy convergence indicator and basis size along the LATIN iterations. In this case, the evolution of the PGD basis along the iterations is different from the LATIN-PGD(θ). More modes are created in the first iterations, where the LATIN convergence indicator rate is higher and there is a large variation in the solution from one iteration to another. Afterwards, the contact quantities converge locally slowly and for several LATIN iterations there is no need to enrich the ROB. The LATIN indicator behaves accordingly. A perfect match in the first part of the convergence curve with respect to the full LATIN indicator, and a very good match in the second part. Remarkably, the size of the PGD basis remains limited, and the final size is in the range of the one obtained previously by means of the LATIN-PGD(θ)+D strategy, which corresponds to the range in which the contact forces are accurately approximated (**Figure 5a**). The progressively built PGD basis, in this case, is not correlated with the SVD, as it can be seen from **Figure 15b** for the auxiliary mixed modes $\{\underline{L}_k\}$. However, it can be noticed that the very first modes have a good correspondence with the first structural modes of the SVD, while subsequent ones, more related to local corrections, are more dispersed and harder to capture optimally. This is because, in the analyzed case, a monostructure case $\Omega_E = \Omega$ was considered and, as seen in **Section 2**, higher-order modes carry localized corrections in different areas of the structure according to sticking/sliding conditions. As

suggested in [35], a multiscale strategy may be useful in this context, with the coarse/macroscale problem quickly capturing the solution at the global scale, and the model-order reduction technique (here PGD) then being able to capture microscopic/local variations in the solution more effectively. This will be illustrated in the next section, where a multiscale strategy based on DDM is proposed within the framework of the LATIN method.

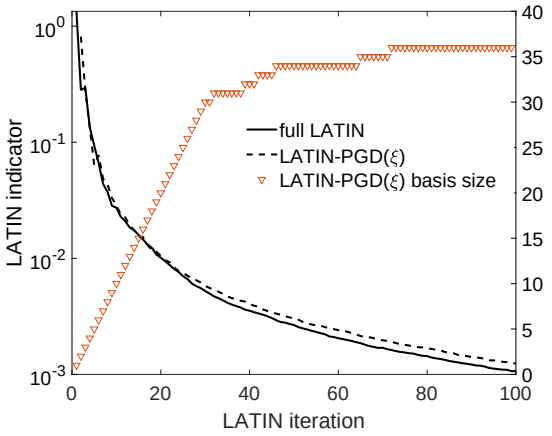

(a) LATIN convergence indicator and the PGD basis size throughout the iterations for the LATIN-PGD(ξ) strategy.

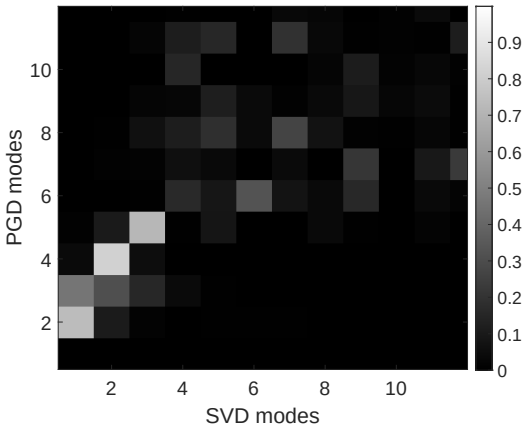

(b) MAC correlation matrix for auxiliary mixed modes $\{\underline{L}_k\}$ for the LATIN-PGD(ξ) strategy.

Figure 15: Convergence curve and PGD basis analysis for the LATIN-PGD(ξ) strategy.

5. Introduction of a multiscale strategy

In this section, the main features of the multiscale strategy are recalled, for further details the interested reader can refer to [23, 56]. The multiscale strategy is introduced in space at the interface level, where the interface unknowns (interface displacements and forces) are additively split into $\square = \square^M + \square^m$ (prior to any discretization), with $\square^M$ being the set of macroscopic quantities and $\square^m$ the complementary set of microscopic ones. The macroscale is defined by the characteristic length of the interfaces, which is a priori greater than the discretization on the microscale. Let us consider an interface $\Gamma_{EE'}$, one may freely choose the spaces $\mathcal{F}_{EE'}^{[0,T],M}$ and $\mathcal{W}_{EE'}^{[0,T],M}$ in which the macroforces and macrodisplacements are sought, provided that these spaces are compatible with the work bilinear form [22, 56]

$$(\underline{W}, \underline{F}) \mapsto \int_{\Gamma_{EE'}\times[0,T]} \underline{F} \cdot \underline{W} \mathrm{d}S\,\mathrm{d}t. \tag{17}$$

Once these spaces are chosen, the macroquantities are provided by:

Definition 12. The macroquantities $(\underline{W}^M, \underline{F}^M) \in \mathcal{W}_{EE'}^{[0,T],M} \times \mathcal{F}_{EE'}^{[0,T],M}$ of $(\underline{W}, \underline{F}) \in \mathcal{W}_{EE'}^{[0,T]} \times \mathcal{F}_{EE'}^{[0,T]}$ are defined by the following expressions:

$$\underline{W}^M \in \mathcal{W}_{EE'}^{[0,T],M},\ \int_{\Gamma_{EE'}\times[0,T]} (\underline{W}^M - \underline{W}) \cdot \underline{F}^{M*} \mathrm{d}S\,\mathrm{d}t = 0,\ \forall \underline{F}^{M*} \in \mathcal{F}_{EE'}^{[0,T],M},$$

$$\underline{F}^M \in \mathcal{F}_{EE'}^{[0,T],M},\ \int_{\Gamma_{EE'}\times[0,T]} (\underline{F}^M - \underline{F}) \cdot \underline{W}^{M*} \mathrm{d}S\,\mathrm{d}t = 0,\ \forall \underline{W}^{M*} \in \mathcal{W}_{EE'}^{[0,T],M}.$$

Consequently, the microquantities are given by $\underline{F}^m = \underline{F} - \underline{F}^M$ and $\underline{W}^m = \underline{W} - \underline{W}^M$, and they are uncoupled in the

following energetic sense:

$$\int_{\Gamma_{EE'}\times[0,T]} \underline{F}\cdot\underline{W}\mathrm{d}S\,\mathrm{d}t = \int_{\Gamma_{EE'}\times[0,T]} \underline{F}^M\cdot\underline{W}^M\mathrm{d}S\,\mathrm{d}t + \int_{\Gamma_{EE'}\times[0,T]} \underline{F}^m\cdot\underline{W}^m\mathrm{d}S\,\mathrm{d}t.$$

This partitioning, extended to the whole set of interfaces, leads to spaces $\mathcal{W}^{[0,T],M}, \mathcal{W}^{[0,T],m}, \mathcal{F}^{[0,T],M}, \mathcal{F}^{[0,T],m}$.

Usually one chooses for $\underline{F}^M$ and $\underline{W}^M$ affine functions in space variable over $\Gamma_{EE'}$, with the only constraint being for the space of the macrodisplacements to include the rigid body modes over $\partial\Omega_E$, so that the multiscale approach is numerically scalable [22, 62]. Finally, $\underline{F}^M$ and $\underline{W}^M$ can be written over $\Gamma_{EE'}$ as $\square^M = \sum_{i=1}^{n_M}(\int_{\Gamma_{EE'}}\square\cdot\underline{e}_i^M(\underline{x})\mathrm{d}S)\underline{e}_i^M(\underline{x})$. A classical choice of affine macrobasis functions $\{\underline{e}_i^M(\underline{x})\}_{i=1,\dots4}$ is represented in **Figure 16** for a 2D straight interface, it contains the rigid body motions of the interface (two translations and rotation) and the linear elongation of the interface [22, 62]. These quantities are mean values with regard to space and enable to represent in particular interface rigid body modes and resultants and moments at the interfaces.

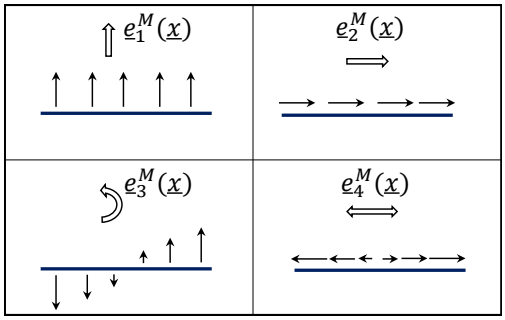

Figure 16: Affine macrobasis $\{\underline{e}_i^M(\underline{x})\}_{i=1,\dots,4}$ ($n_M = 4$) for an interface $\Gamma_{EE'}$.

The key feature of the multiscale strategy is that the equilibrium conditions at the interfaces are required to be verified a priori in a macrosense [22, 56]. The macroforces must be balanced at the interfaces, including the interfaces with boundary conditions. The corresponding space is designated by $\mathcal{F}_{\text{ad}}^{[0,T],M}$, and represents the admissibility of $\underline{F}^M$:

$$\mathcal{F}_{\text{ad}}^{[0,T],M} := \left\{\underline{F}^M \in \mathcal{F}^{[0,T],M} \mid \forall E\in\mathbf{E},\ \forall E'\in\mathbf{V}_E,\ \underline{F}_E^M + \underline{F}_{E'}^M = \underline{0}\right\}. \tag{18}$$

5.1. The multiscale strategy within the LATIN framework

With reference to the substructured **Problem 2**, the partial verification of the transmission conditions a priori at the interfaces (18) leads now to the following partitioning in the LATIN framework:

$$\mathbf{A}_d^{[0,T]}: \left\| \begin{array}{l} \text{– the } E\text{-admissibility of } \mathbf{s}_E, \forall E\in\mathbf{E} : \mathbf{s}_E \in \mathbf{S}_{E,\text{ad}}^{[0,T]} \text{ (\textbf{Definition 1})} \\ \\ \text{– the admissibility of } \underline{F}^M : \underline{F}^M \in \mathcal{F}_{\text{ad}}^{[0,T],M} \text{ (18)} \end{array} \right.$$

$$\boldsymbol{\Gamma}^{[0,T]}: \left\| \text{– the constitutive behavior of the interfaces (1)} \right.$$

The local stage remains unchanged from the one described in **Problem 3**. One has to solve a local problem in space and time for the whole set of interfaces based on known quantities coming from the linear stage. Conversely, in the linear stage, now the a priori balance of the macroforces (18) must be enforced. The admissibility of $\underline{F}^M \in \mathcal{F}_{\text{ad}}^{[0,T],M}$ is enforced on the search direction equation $\mathbf{E}^-$ by means of a Lagrange multiplier $\widetilde{\underline{W}}^M = \{\widetilde{\underline{W}}_E^M\}_{E\in\mathbf{E}}$ [56]:

$$\forall \underline{F}^* \in \mathcal{F}^{[0,T]},\ \sum_{E\in\mathbf{E}}\int_{\partial\Omega_E\times[0,T]} \{\boldsymbol{k}^{-1}(\underline{F}_E - \widehat{\underline{F}}_E) + (\underline{W}_E - \widehat{\underline{W}}_E)\}\cdot\underline{F}_E^*\mathrm{d}S\,\mathrm{d}t = \sum_{E\in\mathbf{E}}\int_{\partial\Omega_E\times[0,T]} \widetilde{\underline{W}}_E^M\cdot\underline{F}_E^*\mathrm{d}S\,\mathrm{d}t, \tag{19}$$

$$\forall \underline{\widetilde{W}}^{M*} \in \mathcal{W}_{\text{ad},0}^{[0,T],M},\ \sum_{E\in\mathbf{E}} \int_{\partial\Omega_E\times[0,T]} \underline{\widetilde{W}}_E^{M*} \cdot \underline{F}_E \mathrm{d}S\,\mathrm{d}t = \sum_{E\in\mathbf{E}} \int_{\partial\Omega_E\cap\partial_2\Omega\times[0,T]} \underline{\widetilde{W}}_E^{M*} \cdot \underline{F}_d \mathrm{d}S\,\mathrm{d}t. \tag{20}$$

The Lagrange multiplier $\underline{\widetilde{W}}^M$ belongs to the space $\mathcal{W}_{\text{ad},0}^{[0,T],M}$ of macrodisplacements which are continuous at the interfaces and equal to zero on $\partial_1\Omega$. Eq. (19) represents the search direction in a weak sense with enforced admissibility of macroforces, and Eq. (20) expresses the admissibility of macroforces in a weak sense. The admissibility of the macroforces ensures the propagation of global information throughout the whole set of substructures across the interfaces. The strategy is numerically scalable provided that the macroforces can represent the resultants and moments at the interfaces, which is ensured with an affine macrobasis (**Figure 16**). The linear stage can now be reformulated as follows:

Problem 13 (*modified linear stage*)**.** Find $\mathbf{s} = \{\mathbf{s}_E\}_{E\in\mathbf{E}} \in \mathbf{A}_d^{[0,T]}$ verifying, $\forall \underline{x} \in \Omega_E$ and $\forall t \in [0,T]$,

$$\left\| \begin{array}{l} \text{– the } E\text{-admissibility of } \mathbf{s}_E\text{: } \mathbf{s}_E \in \mathbf{S}_{E,\text{ad}} \\ \text{– the modified search direction (19)} \\ \text{– the admissibility of macroforces (20)} \end{array} \right.$$

Taking into account the E-admissibility and the modified search direction, the following linear problem, called *microproblem*, has now to be solved for each substructure:

Problem 14 (*microproblem on a substructure*)**.** Find $(\underline{u}_E, \underline{W}_E) \in \mathbf{E}_{E,\text{ad}}^{[0,T]}$ such that, $\forall (\underline{u}^*, \underline{W}^*) \in \mathbf{E}_{E,\text{ad}}^{[0,T]}$,

$$\int_{\Omega_E\times[0,T]} \boldsymbol{\varepsilon}(\underline{u}_E) : \boldsymbol{K} : \boldsymbol{\varepsilon}(\underline{u}^*)\mathrm{d}\Omega\mathrm{d}t + \int_{\partial\Omega_E\times[0,T]} \boldsymbol{k}\underline{W}_E \cdot \underline{W}^* \mathrm{d}S\,\mathrm{d}t = \int_{\Omega_E\times[0,T]} \underline{f}_{d|\Omega_E} \cdot \underline{u}^* \mathrm{d}\Omega\mathrm{d}t + \int_{\partial\Omega_E\times[0,T]} (\widehat{\underline{F}}_E + \boldsymbol{k}\widehat{\underline{W}}_E + \boldsymbol{k}\underline{\widetilde{W}}_E^M) \cdot \underline{W}^* \mathrm{d}S\,\mathrm{d}t,$$

with $\underline{F}_E = \widehat{\underline{F}}_E + \boldsymbol{k}(\widehat{\underline{W}}_E - \underline{W}_E + \underline{\widetilde{W}}_E^M)$.

The solution of **Problem 14**, associated with substructure Ω_E, depends only on the known quantities $\underline{f}_{d|\Omega_E}$, $\hat{\mathbf{s}}_E$ and the unknown Lagrange multiplier $\underline{\widetilde{W}}_E^M$ over $\partial\Omega_E$. Since the problem is linear, the following proposition holds:

Proposition 15. If $\boldsymbol{K}$ and $\boldsymbol{k}$ are symmetric and positive definite, then **Problem 14**, defined over Ω_E and its boundary $\partial\Omega_E$, has a unique solution such that

$$\underline{F}_E^M = \mathbf{L}_E^F(\underline{\widetilde{W}}_E^M) + \underline{\widehat{F}}_{E,d}^M, \tag{21}$$

where $\underline{\widetilde{W}}_E^M \in \mathcal{W}_E^{[0,T],M}$ and $\underline{\widehat{F}}_{E,d}^M$ depends on $\underline{f}_{d|\Omega_E}$ and $\hat{\mathbf{s}}_E$.

$\mathbf{L}_E^F$ is a linear operator from $\mathcal{W}_E^{[0,T],M}$ onto $\mathcal{F}_E^{[0,T],M}$. It can be interpreted as a homogenized behavior operator over substructure Ω_E which ensures the coupling between the microscale and the macroscale. $\mathbf{L}_E^F$ is in practice evaluated by solving a set of microproblems for a set of loading cases $\underline{\widetilde{W}}_E^M$, with $\underline{f}_{d|\Omega_E}$ and $\hat{\mathbf{s}}_E$ set to zero. If $\boldsymbol{k}$ is constant (and since $\boldsymbol{K}$ is the constant Hookean operator for linear elasticity), $\mathbf{L}_E^F$ can be precomputed offline once and for all before starting the iterative process. Since $\underline{\widetilde{W}}_E^M$ depends on only a few interface kinematic parameters, the calculation of $\mathbf{L}_E^F$ is obtained at relatively low cost [56, 57].

5.1.1. The macroproblem over Ω

The Lagrange multiplier $\underline{\widetilde{W}}^M = \{\underline{\widetilde{W}}_E^M\}_{E\in\mathbf{E}}$ is found by solving a macroproblem (or coarse scale problem) over all the set of interfaces. The weak form of the static admissibility of macroforces (20) and the relation (21) lead to the following displacement formulation of the macroproblem in terms of the Lagrange multiplier $\underline{\widetilde{W}}^M$:

Problem 16 (*macroproblem*)**.** Find $\underline{\widetilde{W}}^M = \{\underline{\widetilde{W}}_E^M\}_{E\in\mathbf{E}} \in \mathcal{W}_{\text{ad},0}^{[0,T],M}$ which verifies, $\forall \underline{\widetilde{W}}^{M*} \in \mathcal{W}_{\text{ad},0}^{[0,T],M}$,

$$\sum_{E\in\mathbf{E}} \int_{\partial\Omega_E\times[0,T]} \underline{\widetilde{W}}_E^{M*} \cdot (\mathbf{L}_E^F(\underline{\widetilde{W}}_E^M) + \underline{\widehat{F}}_{E,d}^M)\mathrm{d}S\,\mathrm{d}t = \sum_{E\in\mathbf{E}} \int_{\partial\Omega_E\cup\partial_2\Omega\times[0,T]} \underline{\widetilde{W}}_E^{M*} \cdot \underline{F}_d \mathrm{d}S\,\mathrm{d}t. \tag{22}$$

The problem has a unique solution if $mes(\partial_1\Omega) \neq 0$ [57].

The Lagrange multiplier $\underline{\widetilde{W}}^M$ given by the macroproblem is equal to zero at convergence of the LATIN algorithm, when the balance of interface forces is verified. In practice, it tends to zero quickly in the first iterations, where the macroquantities are rapidly made converge. The macroproblem has a size in space of $\sum_{i=1...n_\Gamma} n_M^{(i)}$, with n_Γ being the total number of interfaces and $n_M^{(i)}$ being the number of macroscopic kinematic unknowns (translations, rotations, extensions) for the interface i. Such kinematics belong to specific classes of continua with affine microstructure [63].

Remark 17. The macroscale has been introduced only in the space variable, while no macroscale was considered in time variable. Defining macroquantities for both space and time variables is addressed in [56]. When the strategy is multiscale only in space, the macroproblem must be solved at each time interval of the fine time partition. When the macroproblem becomes very large, this step can become prohibitive in the case of evolution problems with a lot of time steps. Introducing a macroscale in time may then be necessary [56], and possibly model-order reduction to solve the macroproblem [38].

5.1.2. The final algorithm

The final algorithm of the LATIN-based multiscale DDM is shown in **Algorithm 2**. It is an extension of the strategy presented in **Section 3** for the monoscale case. After the local stage (**Problem 3**), local stage quantities $\hat{\mathbf{s}}$ are used as boundary loadings to solve a problem at the substructure scale. This is called *microproblem 1*, coincident with the linear stage problem to be solved in the monoscale case (**Problem 5**). In the multiscale approach, after solving microproblem 1 for each substructure, the macrocomponent $\underline{F}^M$ of the interface forces are extracted and used to solve the macroproblem (**Problem 16**) and to find the Lagrange multiplier $\underline{\widetilde{W}}_E^M$ of each interface, which is used as boundary loading to solve the *microproblem 2*. Thus, the linear stage solution is the sum of the solutions of microproblem 1 and microproblem 2.

5.2. Resolution of microproblems with PGD

The introduction of PGD in the multiscale approach to solve the two microproblems is entirely analogous to what was presented in **Section 4** for the monoscale case. Starting from an admissible initial solution $\mathbf{s}_0$ (**Problem 6**), the current iteration solution can be expressed as a correction with respect to the previous one: $\mathbf{s}_{n+1} = \mathbf{s}_n + \Delta\mathbf{s}$. Therefore, each microproblem of the multiscale strategy can be expressed in terms of corrections as in **Problem 8**, with $\underline{\delta}_{E,1} = \underline{\widehat{F}}_E + \boldsymbol{k}\underline{\widehat{W}}_E - (\underline{F}_{E,n} + \boldsymbol{k}\underline{W}_{E,n})$ for microproblem 1 and $\underline{\delta}_{E,2} = \boldsymbol{k}\underline{\widetilde{W}}_E^M$ for microproblem 2. The two microproblems share the same PGD basis and the procedure is analogous as the one described in **Section 4**, with the only difference that now it is applied to two microproblems. In microproblem 1, an updating of the time modes is operated with the given space modes fixed with **Problem 10** and, if the ξ enrichment criterion (15) is not satisfied, a new pair of modes is added with **Algorithm 1**. Once the first microproblem is solved for each substructure, the macroforces are extracted and the Lagrange multipliers $\underline{\widetilde{W}}^M = \{\underline{\widetilde{W}}_E^M\}_{E\in\mathbf{E}}$ are found through the resolution of the macroproblem (**Problem 16**). Then, one proceeds to solve microproblem 2 by updating the current time modes and eventually adding a new pair of modes if the enrichment criterion is not satisfied.

At the start of the multiscale strategy, convergence is mainly driven by the macroquantities, which converge rapidly in the first iterations. Therefore, it is reasonable to require the macroquantities to be sufficiently well approximated in the early stages of the iterative process, in order to take full advantage of the multiscale strategy. We recall that each microproblem 2 has as a loading the Lagrange multiplier $\underline{\widetilde{W}}_E^M$ on the boundary $\partial\Omega_E$, and that $\underline{\widetilde{W}}_E^M$ belongs to a finite-dimensional space of small size. Therefore, a small finite number of modes is sufficient to precisely solve microproblem 2 over all the iterations. For this reason, it is reasonable to require a bit more strict enrichment criterion threshold $\xi_{0,2}$ for microproblem 2 (e.g., $\xi_{0,2} = 0.01$), and a bit coarser enrichment criterion threshold for microproblem 1 (e.g., $\xi_{0,1} = 0.1$). Consequently, at the beginning of the iterations, the algorithm tends to generate systematically more modes arising from microproblem 2, so that macroquantities converge quickly and accurately. Thereafter, once a sufficient basis has been formed for the macroquantities, in the following iterations most of the generated modes will be generated from microproblem 1, which converges more slowly and brings more localized corrections.

It is clear that with such a strategy, based on the physics of the problem, the algorithm naturally tends to generate macro/coarse modes due to the macroproblem and microproblem 2, and bring local refinements with modes generated from microproblem 1. Orthonormality criteria and sorting and downsizing methods are therefore not very natural in this case since the two microproblems already reflect corrections from different scales, as shown in the following.

Algorithm 2: Multiscale LATIN-DDM

■ **preliminary computations**

for each substructure Ω_E **do**

– compute the homogenized operator $\mathbf{L}_E^F$

– initialize admissible solution $\mathbf{s}_{0,E}$ (**Problem 6**)

■ **LATIN iterations**

for $n = 1$ to $n_{\max}$ **do**

■ **local stage**: find $\hat{\mathbf{s}}_{n+1/2} \in \mathbf{\Gamma}^{[0,T]}$

for each interface $\Gamma_{EE'}$ **do**

– solve interface **Problem 3** to find $\hat{\mathbf{s}}_E = (\widehat{\underline{W}}_E, \widehat{\underline{F}}_E)$ (see Appendix A)

– set $\hat{\mathbf{s}}_{n+1/2} = \{\hat{\mathbf{s}}_E\}_{E\in\mathbf{E}}$

■ **linear stage**: find $\mathbf{s}_{n+1} \in \mathbf{A}_d^{[0,T]}$

■ **microproblem 1**

for each substructure Ω_E **do**

– find $(\hat{\underline{u}}_{E,d}, \widehat{\underline{W}}_{E,d}) \in \mathbf{E}_{E,\mathrm{ad}}^{[0,T]}$ such that, $\forall (\underline{u}^*, \underline{W}^*) \in \mathbf{E}_{E,\mathrm{ad}}^{[0,T]}$,

$$\int_{\Omega_E\times[0,T]} \boldsymbol{\varepsilon}(\hat{\underline{u}}_{E,d}) : \boldsymbol{K} : \boldsymbol{\varepsilon}(\underline{u}^*)\mathrm{d}\Omega\mathrm{d}t + \int_{\partial\Omega_E\times[0,T]} \boldsymbol{k}\widehat{\underline{W}}_{E,d} \cdot \underline{W}^*\mathrm{d}S\,\mathrm{d}t = \int_{\Omega_E\times[0,T]} \underline{f}_{d|\Omega_E} \cdot \underline{u}^*\mathrm{d}\Omega\mathrm{d}t + \int_{\partial\Omega_E\times[0,T]} (\widehat{\underline{F}}_E + \boldsymbol{k}\widehat{\underline{W}}_E) \cdot \underline{W}^*\mathrm{d}S\,\mathrm{d}t$$

– find $\widehat{\underline{F}}_{E,d}$ through the search direction $\mathbf{E}^-$: $\widehat{\underline{F}}_{E,d} - \widehat{\underline{F}}_E + \boldsymbol{k}(\widehat{\underline{W}}_{E,d} - \widehat{\underline{W}}_E) = \underline{0}$

– compute macroforces $\widehat{\underline{F}}_{E,d}^M$

– set $\mathbf{s}_{n+1} = \{\hat{\mathbf{s}}_{E,d}\}_{E\in\mathbf{E}}$

if multiscale **then**

■ **macroproblem**:

– find $\widetilde{\underline{W}}^M = \{\widetilde{\underline{W}}_E^M\}_{E\in\mathbf{E}} \in \mathcal{W}_{\mathrm{ad},0}^{[0,T],M}$ such that, $\forall \widetilde{\underline{W}}^{M*} \in \mathcal{W}_{\mathrm{ad},0}^{[0,T],M}$,

$$\sum_{E\in\mathbf{E}} \int_{\partial\Omega_E\times[0,T]} \widetilde{\underline{W}}_E^{M*} \cdot (\mathbf{L}_E^F(\widetilde{\underline{W}}_E^M) + \widehat{\underline{F}}_{E,d}^M)\mathrm{d}S\,\mathrm{d}t = \sum_{E\in\mathbf{E}} \int_{\partial\Omega_E\cup\partial_2\Omega\times[0,T]} \widetilde{\underline{W}}_E^{M*} \cdot \underline{F}_d^M\mathrm{d}S\,\mathrm{d}t$$

■ **microproblem 2**

for each substructure Ω_E **do**

– find $(\tilde{\underline{u}}_E, \widetilde{\underline{W}}_E) \in \mathbf{E}_{E,\mathrm{ad}}^{[0,T]}$ such that, $\forall (\underline{u}^*, \underline{W}^*) \in \mathbf{E}_{E,\mathrm{ad}}^{[0,T]}$,

$$\int_{\Omega_E\times[0,T]} \boldsymbol{\varepsilon}(\tilde{\underline{u}}_E) \;:\; \boldsymbol{K} \;:\; \boldsymbol{\varepsilon}(\underline{u}^*)\mathrm{d}\Omega\mathrm{d}t + \int_{\partial\Omega_E\times[0,T]} \boldsymbol{k}\widetilde{\underline{W}}_E \cdot \underline{W}^*\mathrm{d}S\,\mathrm{d}t = \int_{\partial\Omega_E\times[0,T]} \boldsymbol{k}\widetilde{\underline{W}}_E^M \cdot \underline{W}^*\mathrm{d}S\,\mathrm{d}t$$

– find $\widetilde{\underline{F}}_E$ through the search direction $\mathbf{E}^-$: $\widetilde{\underline{F}}_E + \boldsymbol{k}(\widetilde{\underline{W}}_E - \widetilde{\underline{W}}_E^M) = 0$

– set $\tilde{\mathbf{s}}_{n+1} = \{\tilde{\mathbf{s}}_E\}_{E\in\mathbf{E}}$

– update $\mathbf{s}_{n+1} \leftarrow \mathbf{s}_{n+1} + \tilde{\mathbf{s}}_{n+1}$

– apply relaxation: $\mathbf{s}_{n+1} \leftarrow \mu\mathbf{s}_{n+1} + (1-\mu)\mathbf{s}_n$

– compute error indicator η (3)

5.3. Application to the test problem

The multiscale strategy is applied here to the 1D test problem. Substructured cases are considered, as in **Figure 11**. In **Figure 17** is shown, for different number of substructures, the behavior of the LATIN indicator η in the monoscale version and in the multiscale one, without resorting to PGD. The multiscale approach allows for a considerable convergence gain in the first iterations, where macroquantities are rapidly converged. Subsequently, contact quantities

are converged to the local microlevel. In this second stage, the monoscale and multiscale approach exhibit roughly the same convergence rate since both of them are making converge the quantities at the microlevel, and the convergence rate at the microlevel is mainly driven by the search direction $\boldsymbol{k}$. To highlight the effect of the multiscale strategy

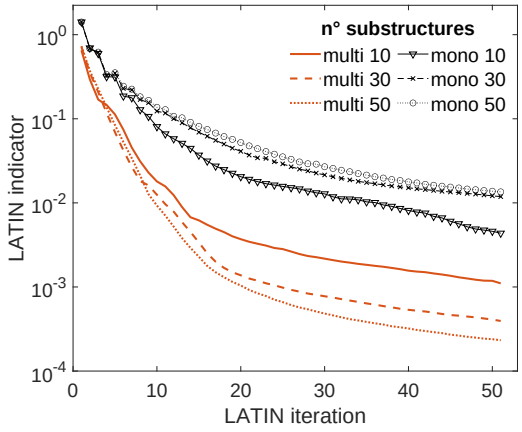

Figure 17: Monoscale and multiscale LATIN convergence indicator for different number of substructures.

on the solution of the problem, in **Figure 18** is shown, in the case of 10 substructures, the solution for the frictional forces after 10 iterations of the LATIN method for the monoscale approach and the multiscale one, compared to the reference solution at time $t = 0.5$ s (**Figure 18a**) and $t = 1$ s (**Figure 18b**). Already after few iterations, the multiscale approach succeeds in capturing the global behavior of the problem. Subsequently, further iterations are needed to make converge the microquantities, especially at the sticking-sliding discontinuity zones which need accurate local refinements. The monoscale approach, on the other hand, turns out to be far from the reference solution, with the loading boundary condition still not fully propagated along all the substructures.

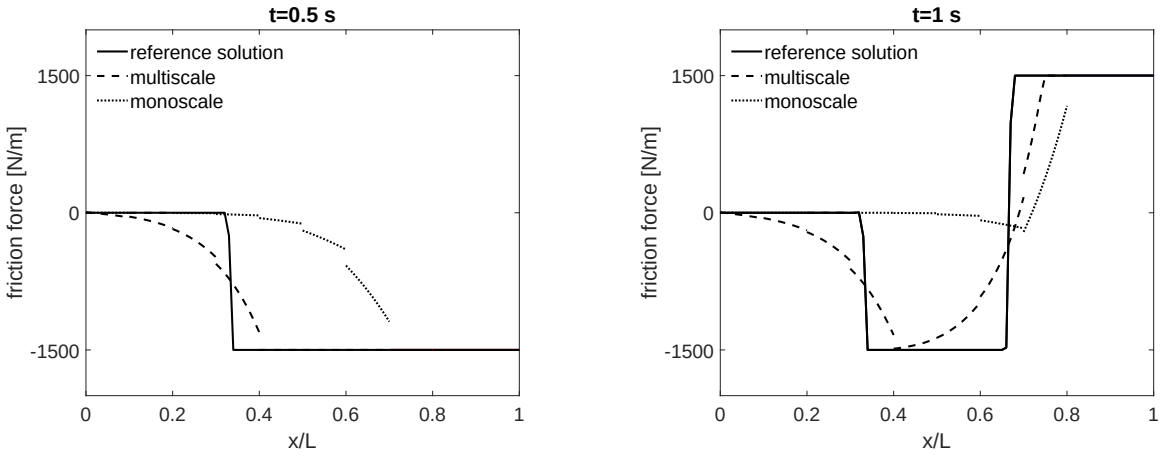

(a) Frictional forces distribution at time $t = 0.5$ s.

(b) Frictional forces distribution at time $t = 1$ s.

Figure 18: Frictional forces distribution after 10 iterations of the full LATIN (without PGD) for the monoscale and the multiscale approach.

The effect of introducing PGD in the multiscale approach is shown in **Figure 19**. By making use of DDM, one is able to create local reduced bases per substructure and enrich the basis in the areas with more complex contact conditions, as exemplified in **Figure 4**. In **Figure 19a**, in the case of 5 substructures, is shown the evolution of the

PGD basis size for different substructures. An enrichment threshold $\xi_{0,1} = 0.1$ for microproblem 1, and $\xi_{0,2} = 0.01$ for microproblem 2 was adopted. Different substructures require a different number of modes. For substructure 1, constantly under sticking conditions, the macrobasis is sufficient to capture the solution. Subsequent substructures, on the other hand, require more modes based on the complexity of the sticking-sliding conditions. What is important to remark is that the PGD basis remains in fact limited in size and, in addition, the MAC diagram in **Figure 19b** shows that the first structural modes are roughly well captured by the macroproblem.

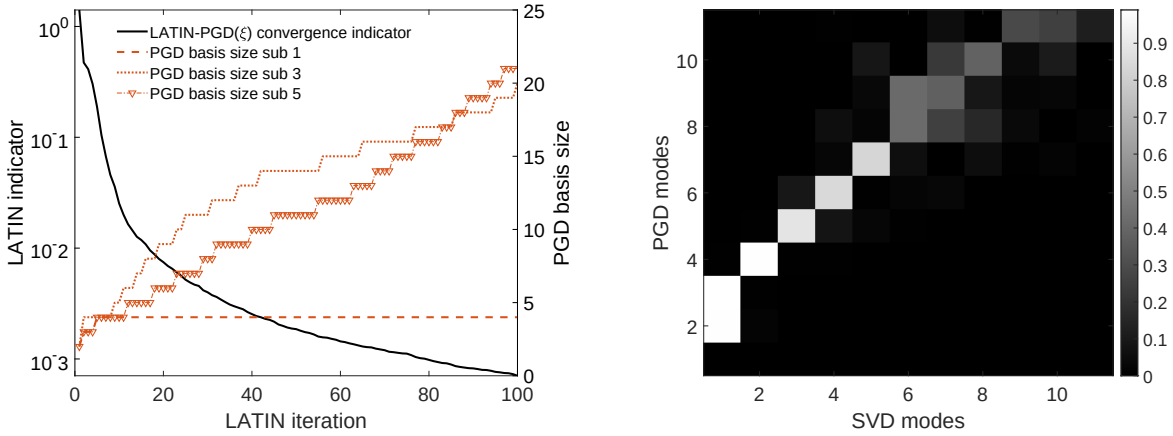

(a) LATIN indicator and PGD basis size per substructure.

(b) MAC diagram for mixed modes $\{\underline{L}_k\}$ of substructure 5.

Figure 19: Convergence curve and PGD basis analysis for the multiscale LATIN-PGD(ξ) strategy.

6. A 2D numerical application

6.1. Problem setting and analysis of the solution

In this section, the multiscale strategy is applied to the two-dimensional quasistatic frictional contact problem depicted in **Figure 20a**. The problem consists of a group of three clamped beams subjected to a constant external pressure p and to time-dependent oscillating traction and shear (which causes bending) loads in correspondence of the free side. Each beam is decomposed internally into 6 substructures, and they are in contact with each other through frictional contact interfaces. The external pressure is constant and equal to 100 MPa, while the external loads evolution in time is represented in **Figure 20b**. The parameters of the problem are reported in **Table 3**. Plain strain assumptions are considered, and 8-node quadrilateral elements (QUA8) are adopted for the discretization of the substructures. For the discretization of interface quantities, on the other hand, piecewise constant elements are adopted while satisfying the LBB condition [23]. A reference search direction parameter $k = E/L_\Gamma$ was chosen for each interface, with L_Γ being the length of the interface. The test case can be seen as representative of structures with multiple contact interfaces subjected to oscillating traction and bending loads, such as wire ropes for offshore applications [2, 37]. These kind of structures require an accurate computation of local contact quantities for fretting fatigue life prediction [64].

The reference solution is here obtained with the full multiscale LATIN method, for a convergence indicator value of $\eta = 1.5 \cdot 10^{-5}$. In **Figure 22** is shown the trend of the tangential frictional forces and their macroscopic part at time instant A ($t = 0.5$ s) along the contact interface Γ_c highlighted in **Figure 20a**, which goes along the entire length of the structure. As it can be seen, the affine macroscopic part roughly captures the trend of forces on each interface. In **Figure 23** is shown the relative sliding along Γ_c, at time instants A ($t = 0.5$ s) and B ($t = 1.5$ s). In A, where minimum bending occurs, almost the entire structure results in a sticking state. The sliding is confined near the clamped boundary, between substructures 1 and 7. In B, corresponding to maximum bending, on the other hand, the whole contact interface turns out to be in a sliding state. In this case, the sliding propagates through the substructures. Sliding fronts

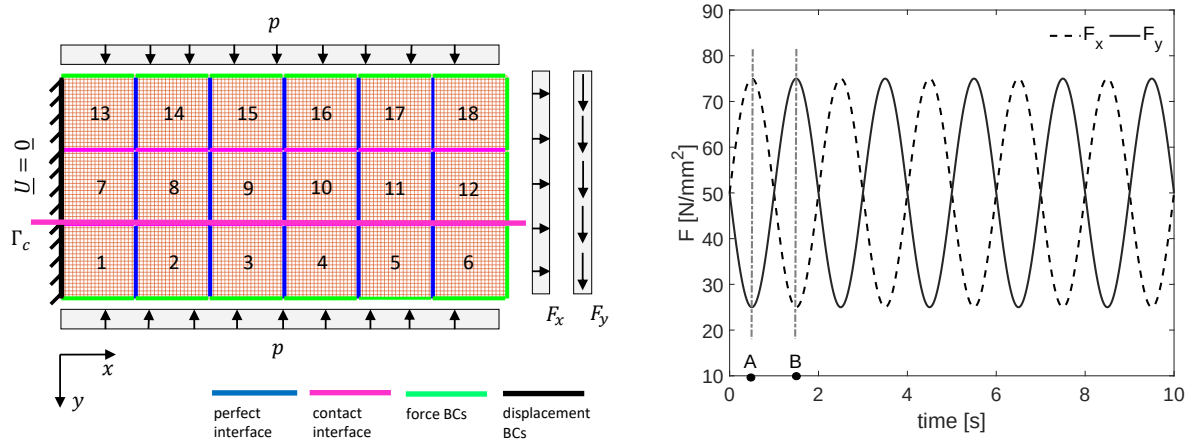

(a) Representation of substructures and interfaces, with numbering of the substrcture. Highlight of the contact interface Γ_c between two beams.

(b) Time evolution of prescribed external forces. Highlight of time instants A (t = 0.5 s) and B (t = 1.5 s).

Figure 20: Two-dimensional problem.

Parameters of the 2D problem	
Young modulus, E	130,000 MPa
Poisson ratio, ν	0.2
structure size L_x, L_y	180, 90 mm
number of elements per substructure	20×20 QUA8
number of DOFs per substructure, N_x	2562
number of time steps, N_t	1000
time interval, $[0, T]$	[0, 10 s]
friction coefficient, f	0.3
pressure load, p	100 MPa

Table 3: Parameters for the two-dimensional problem.

propagating through all the substructures can affect the relevance of the coarse scale **Problem 16**. The evolution of the LATIN indicator in **Figure 21**, shows that there is in fact an initial gain in convergence, where boundary conditions and macroquantities are propagated throughout the whole structure. However, thereafter the convergence rate turns out to be comparable to the monoscale one. Since the macroproblem is based on the balance of macroforces, in a problem where a large sliding/discontinuity front propagates through the substructures, the macroproblem after a certain point brings few contribution on the solution of the contact problem locally, and iterating more is necessary [43, 44].

The convergence state of the contact quantities coming from the linear and local stage (normal and tangential forces and displacements) along the iterations of the multiscale full LATIN, at the contact interface $\Gamma_{c,1-7}$ between substructures 1 and 7, is shown in **Figure 24** for the time instant A of the loading. After 100 iterations, and a LATIN indicator value of $\eta = 4 \cdot 10^{-4}$, the structure results are far from convergence. Regarding contact forces, the quantities coming from the local stage appear to have already identified the sticking and sliding zones. This means that the contact status, thanks to the multiscale approach, has converged quickly. As it can be seen in the next iterations, 500 ($\eta = 8 \cdot 10^{-5}$) and 1000 ($\eta = 1.5 \cdot 10^{-5}$), the forces from the local stage identify roughly the same sticking-sliding transition zones. However, the tangential forces of the linear stage turn out to converge very slowly toward this threshold of sticking-sliding. In contrast, the normal forces result to converge more rapidly. This fact may be due to the choice of search direction parameter $\boldsymbol{k}$. Tangential contact and normal contact should require different stiffness

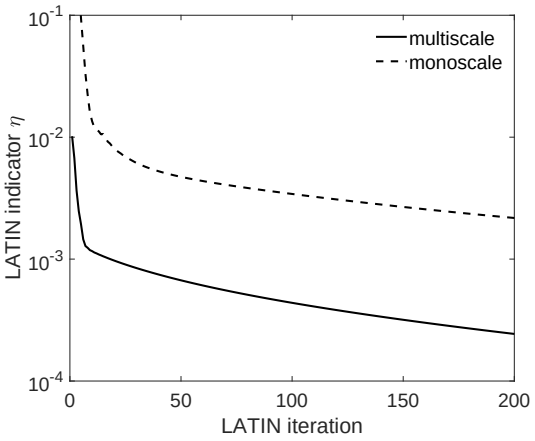

Figure 21: LATIN indicator of the multiscale approach compared to the monoscale one for the 2D problem.

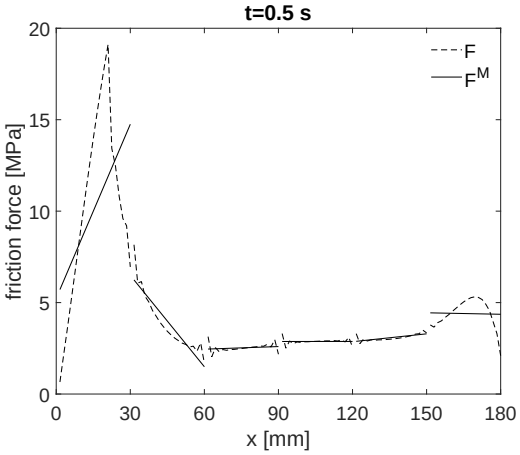

Figure 22: Spatial distribution of the frictional forces and their macropart along Γ_c at time instant A.

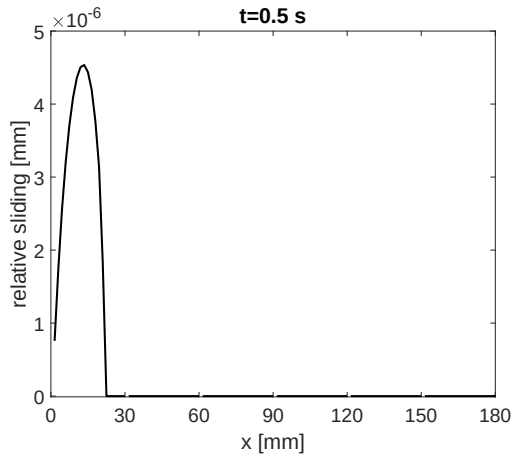

(a) Sliding at time instant A.

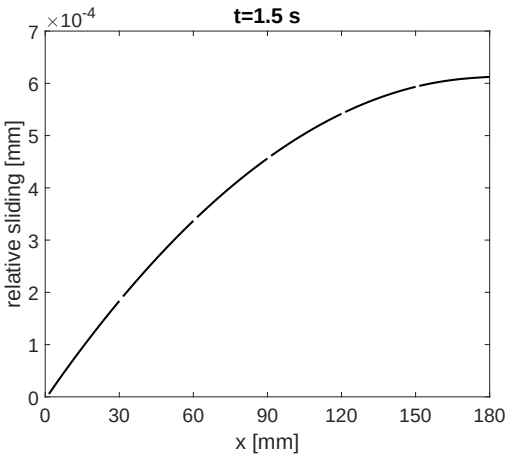

(b) Sliding at time instant B.

Figure 23: Relative sliding along the contact interface Γ_c at time instants A and B.

[55]. In the case of normal contact, under closed gap conditions, the stiffness can be considered as the one of perfect interfaces. In the case of tangential contact, on the other hand, more prone to slippage, the contact stiffness should be lowered. As a result, convergence can be very slow in specific areas where sliding occurs. Optimizing and updating the search direction for this class of problems requires further study and will be covered in a later article.

6.2. Introduction of PGD

6.2.1. Influence of the choice of the PGD enrichment criterion

The introduction of PGD is performed at the substructure level, with the enrichment criterion of Eq. (15) which takes into account the approximation on the search direction. **Figure 25a** shows the evolution of the LATIN indicator in the multiscale full LATIN case and in the case of the LATIN-PGD(ξ) strategy with different enrichment thresholds. A very strict enrichment threshold of $\xi_{0,1} = \xi_{0,2} = 10^{-4}$ for both microproblems leads the LATIN-PGD(ξ) convergence curve to coincide with the full LATIN curve, since at each iteration the search direction is approximated with very good accuracy. A very coarse enrichment threshold, such as $\xi_{0,1} = \xi_{0,2} = 0.5$ on both microproblems, on the other

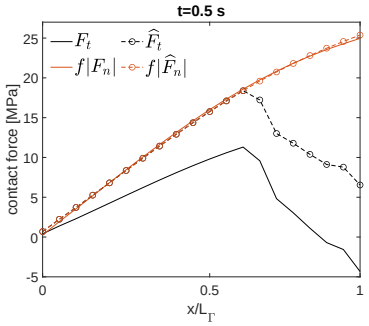

(a) Normal and tangential forces at iteration 100.

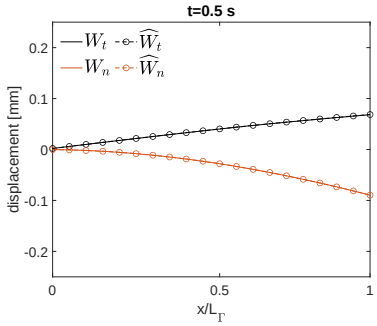

(b) Normal and tangential displacements at iteration 100.

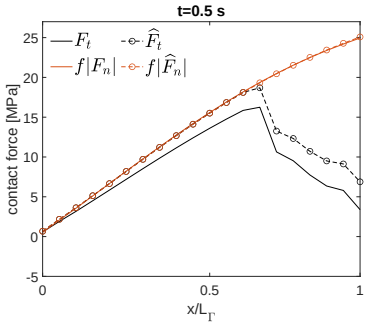

(c) Normal and tangential forces at iteration 500.

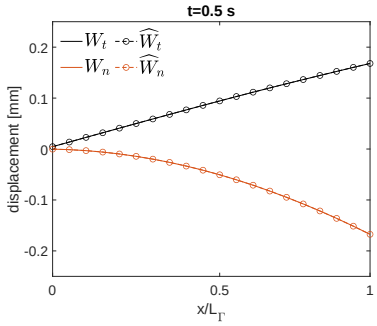

(d) Normal and tangential displacements at iteration 500.

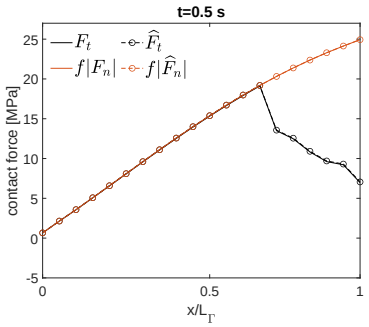

(e) Normal and tangential forces at iteration 1000.

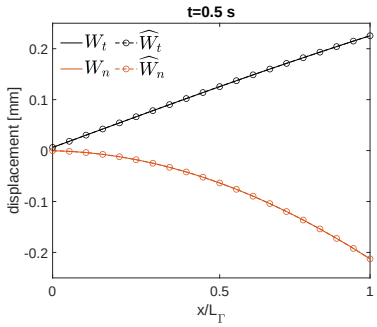

(f) Normal and tangential displacements at iteration 1000.

Figure 24: Convergence state of normal (in red) and tangential (in black) forces and displacements at time instant A for interface $\Gamma_{c,1-7}$ through the LATIN iterations.

hand, leads the solution to stagnate and risk diverging. The initial part of the curve is not properly approximated, which leads to affect the convergence in the rest of the iterations. By making use of a different enrichment threshold for the two microproblems, as explained in **Section 5.2**, that is, a bit more strict for microproblem 2 ($\xi_{0,2} = 0.01$), and a bit coarser for microproblem 1 ($\xi_{0,1} = 0.1$), leads to a good approximation of the problem. In fact, it is not important to correctly approximate the search direction at each iteration, as it is useless when the algorithm is still far from convergence. The important thing is to approximate the problem sufficiently to stay close to the convergence given by the full LATIN (which, in fact, is the best that can be done with a given search direction $\boldsymbol{k}$), while trying to generate as few modes as possible.

In **Figure 25b** is shown the evolution of the PGD basis size along the LATIN iterations in two different substructures for two choices of the enrichment threshold, that is $\xi_{0,1} = \xi_{0,2} = 10^{-4}$ and $\xi_{0,1} = 0.1$, $\xi_{0,2} = 0.01$. The considered substructures are substructure 7 and substrcture 12. The former is located in the clamped zone, and features edge

effects that make the contact conditions more difficult to capture. It is therefore expected that a higher number of modes will be required compared to substructure 12.

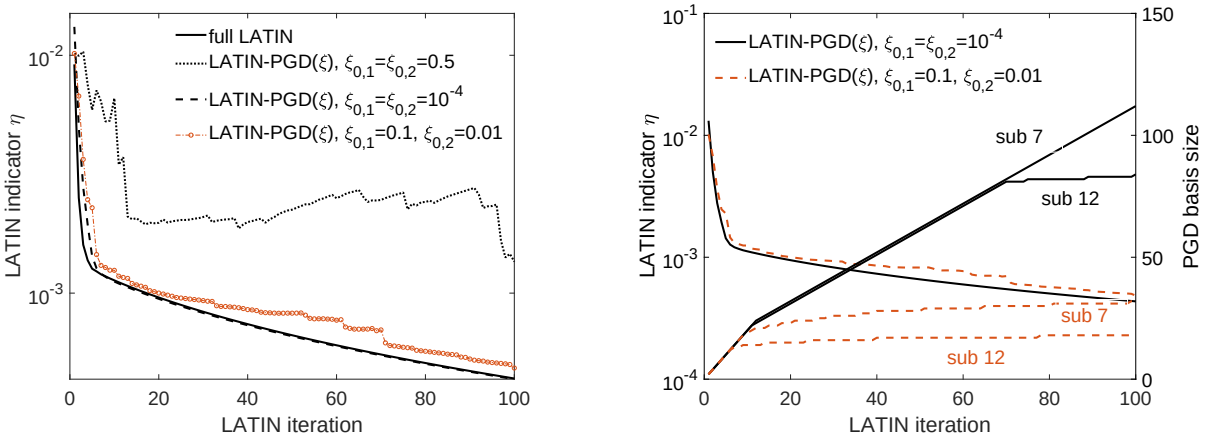

(a) LATIN convergence indicator of full LATIN and LATIN-PGD(ξ).

(b) PGD basis size along the iterations for the LATIN-PG(ξ) strategy.

Figure 25: Convergence curves and PGD basis size for the multiscale LATIN-PGD(ξ) strategy.

Both choices systematically generate two pairs of modes, one from each microproblem, in the first iterations, where the slope of the LATIN curve is higher. Thereafter, in the case with $\xi_{0,1} = \xi_{0,2} = 10^{-4}$, only one pair of modes, coming from microproblem 1, is generated systematically at each iteration for both substructures. In fact, as explained in **Section 5.2**, a relevant basis of small size for microproblem 2, related to macroquantities, has been generated in the first iterations, where macroquantities are quickly made converge. Therefore, after the first iterations, there is no need for microproblem 2 to generate new modes and the updating of time modes (see **Problem 10**) is sufficient. In contrast, for microproblem 1, related to microquantities, it is necessary to enrich the basis frequently. However, as mentioned previously, it is not strictly necessary to correctly approximate microproblem 1 from the beginning, since it converges slowly. Accordingly, with the choice of $\xi_1 = 0.1$ and $\xi_2 = 0.01$, a relevant basis for microproblem 2 is generated in the first iterations. Thereafter new modes are generated sporadically when needed only for the microproblem 1, thus reducing the size of the final basis.

The accuracy of the contact quantities for the two enrichment threshold choices described above are shown in **Figure 26** for the contact forces along interface $\Gamma_{c,1-7}$ at time instant A. When the search direction is well approximated, as in the case of $\xi_{0,1} = \xi_{0,2} = 10^{-4}$, the solution coincides in practice with the full LATIN solution at each iteration, and a large number of modes is required. In the other case, the approximation becomes better as one approaches the converged solution where the two strategies are indistinguishable. Nevertheless, the difference in the size of the PGD basis built by the two strategies per substructure, as it can be seen from **Figure 25b**, is of a factor of 4.

6.2.2. Analysis of the computational cost

It is also crucial to quantify the gain in computational time that adopting PGD brings to the LATIN algorithm, based on the choices of the enrichment criterion threshold and possible algorithms to control the size and quality of the progressively built PGD basis. The average computational time (over 100 iterations) of the linear stage of the LATIN-PGD(ξ) and LATIN-PGD(ξ)+D strategies (see **Table 2**), with the two choices of enrichment criteria described previously, is shown in **Figure 27**. Concerning the LATIN-PGD(ξ), undoubtedly a criterion that creates fewer PGD modes is less expensive, and saves up to 40% of the time in this case. Compared with the the full LATIN, the LATIN-PGD(ξ) allows a gain of a factor larger than 10.

In the LATIN-PGD(ξ)+D strategy with $\xi_{0,1} = \xi_{0,2} = 10^{-4}$, which leads to the generation of a large number of modes (see **Figure 25b**), the downsizing stage turns out to be very expensive, with the cost associated with the satisfaction of the admissibility condition (10) for the separated representation of interface quantities each time the

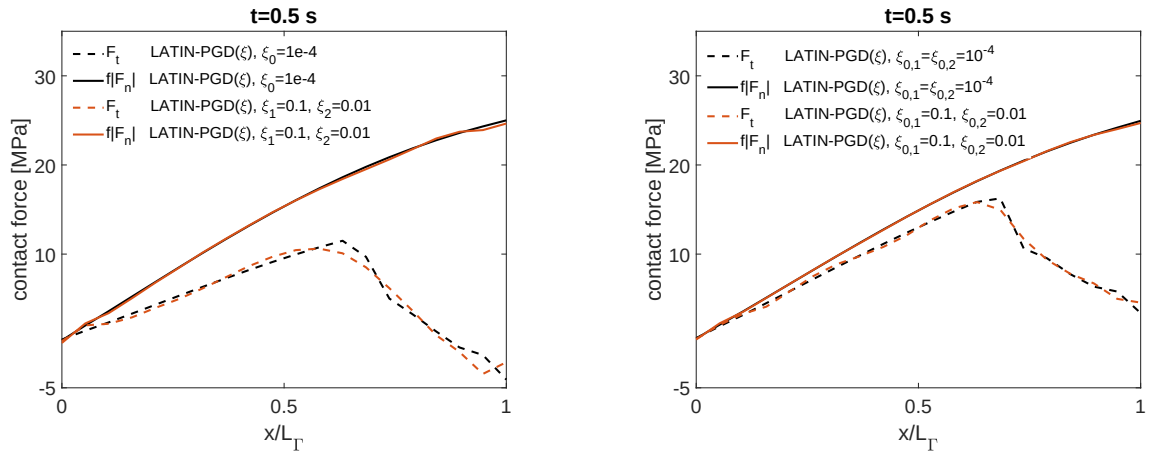

(a) Linear stage normal and tangential forces at iteration 100.

(b) Linear stage normal and tangential forces at iteration 500.

Figure 26: Linear stage normal and tangential forces at time instant A for interface $\Gamma_{c,1-7}$ for the LATIN-PGD(ξ) strategy at two different number of iterations.

downsizing stage is applied. Its overall computational cost becomes therefore comparable with the cost of the full LATIN, leading to a very low gain in computational time. Instead, when in the LATIN-PGD(ξ)+D a more appropriate threshold is chosen ($\xi_{0,1} = 0.1$ and $\xi_{0,2} = 0.01$), performing downsizing becomes less costly, as less modes are generated, yet still the cost is non-negligible.

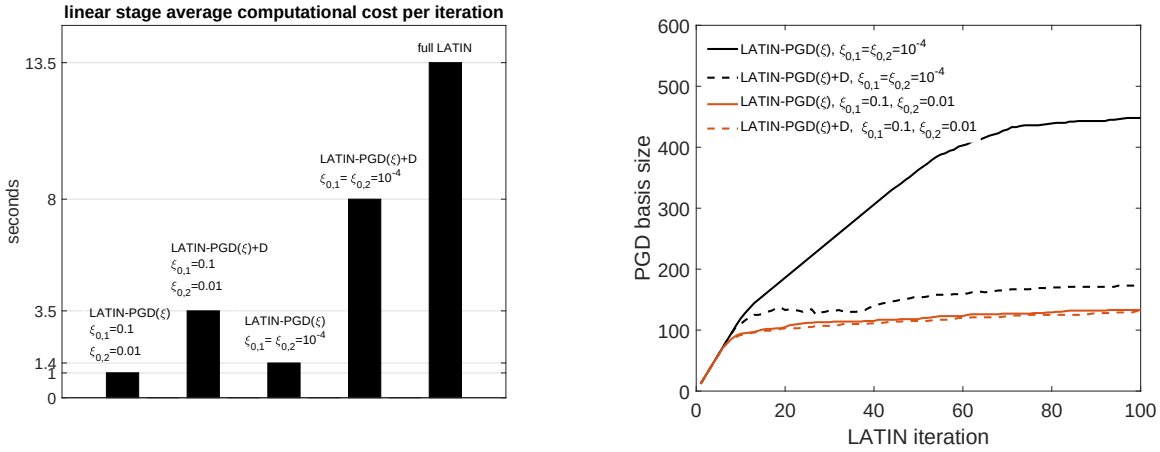

(a) Computational cost of LATIN-PGD(ξ), LATIN-PGD(ξ)+D and full LATIN.

(b) PGD basis size of LATIN-PGD(ξ) and LATIN-PGD(ξ)+D.

Figure 27: LATIN-PGD(ξ)+D strategy computational cost and basis size.

The influence of a downsizing stage on the size of the PGD reduced basis is shown in **Figure 27b**, where the evolution of the size of the total basis for substructures 7 to 12 of the central beam of **Figure 20a** is plotted. In the LATIN-PGD(ξ) strategy with $\xi_{0,1} = \xi_{0,2} = 10^{-4}$, the size of the progressively built reduced basis is remarkably large. In this case, downsizing significantly reduces the size by sorting and taking out unnecessary modes, however, at a non-negligible computational cost. In the case of LATIN-PGD(ξ) with $\xi_{0,1} = 0.1$ and $\xi_{0,2} = 0.01$, instead, the redundancy of the progressively found modes is minimal, and the effect and the need of of the downszing stage can be said to be negligible on the final size of the basis.

7. Conclusions and perspectives

A multiscale strategy to model-order reduction for frictional contact problems was discussed in this paper. The multiscale strategy is based on a mixed DDM equipped with a coarse scale problem solved with the LATIN method. PGD-based model reduction is naturally introduced in the LATIN through the separation of variables at the linear stage. The analysis of a simple one-dimensional frictional contact problem brought to light some aspects of this type of problems:

– space modes bring localized corrections on the different sticking-sliding areas, indicating the potential benefit of their a priori separation through a DDM approach to be more accurate locally,

– a large propagation in sliding front drastically decreases reducibility, as also affects the relevance of the coarse scale problem on the convergence speed-up.

In the analyzed 2D problem it was shown how, for a given accuracy, in order to achieve the best efficiency in terms of computational cost reduction it is required to create as few PGD modes as possible. Therefore, the choice of the PGD basis enrichment criterion is crucial. By exploiting the fact that the coarse scale problem brings advantages especially in the first iterations of the LATIN, it is suggested to:

– systematically enrich in the first iterations the ROB due to macroquantities (microproblem 2), so as to form a relevant basis for the macroquantities for the rest of the iterations,

– select a more precautionary enrichment criterion threshold for the microquantites (microproblem 1), whose convergence is much slower especially in problems with large sliding fronts across multiple substructures, so as to not add unnecessarily modes when far from convergence.

The sorting and downsizing algoritm proposed in [35] has been adapted and extended here in the multiscale and DDM version of the LATIN. The algorithm controls the PGD basis size and creates a close-to-optimal basis throughout the computations. However, its computational cost, due to the need to guarantee admissibility between the modes of displacements and forces each time it is applied, is not negligible, especially when using an inappropriate ROB enrichment criterion which leads to add many modes. It was shown that, by making use of the previous suggestions, the need for downsizing can be avoided thanks to the multiscale aspects and the DDM, since the two microproblems already reflect corrections from different scales. In such a way, an important gain in computational time with respect to the full LATIN solver is achieved, and a ROB of controlled size and good quality is progressively created. Modes due to the macroproblem capture the low frequency modes of each subdomain, while those from the microquantities capture progressively modes that carry more local and refined corrections.

In the analyzed 2D problem, the large contact interfaces subjected to sliding along the whole set of substructures affect the solution at the global level over the whole structure, and the coarse scale problem, after an initial convergence gain, reduces its effect and at the microlevel still many iterations are needed. A future perspective to deal with this issue is to resort to contact status-based search direction update techniques, in order to speed up convergence at the microlevel. However, this requires the recomputation of the LATIN linear operators, which may be expensive, as well as a more appropriate convergence indicator which does not depend on the search direction. Moreover, even though a reduced computational time can be achieved for the linear stage with a separated representation, the local stage is still solved in a full format. When a large number of interfaces and many time-steps are present, the local stage may become expensive, especially for frictional contact interfaces which are solved incrementally over time. Another future perspective is thus the possibility to integrate the local stage in a reduced format as well by making use, for example, of an a hyperreduction format dedicated to the LATIN-PGD [65].

Appendix A. Local stage for different interface behaviors

■ Displacement boundary conditions

For a displacement $\underline{U}_d$ imposed on $\Gamma_{E,1} = \partial\Omega_E \cap \partial_1\Omega$, taking into account the search direction, the following conditions have to be imposed:

$$\begin{cases} \widehat{\underline{W}}_E = \underline{U}_d \\ \widehat{\underline{F}}_E = \underline{F}_E + \boldsymbol{k}(\widehat{\underline{W}}_E - \underline{W}_E) \end{cases} \tag{A.1}$$

■ **Force boundary conditions**

For an imposed force $\underline{F}_d$ on $\Gamma_{E,2} = \partial\Omega_E \cap \partial_2\Omega$, taking into account the search direction, the following conditions have to be imposed:

$$\begin{cases} \widehat{\underline{F}}_E = \underline{F}_d \\ \widehat{\underline{W}}_E = \underline{W}_E + \boldsymbol{k}^{-1}(\widehat{\underline{F}}_E - \underline{F}_E) \end{cases} \tag{A.2}$$

■ **Perfect interfaces**

For a perfect interface $\Gamma_{EE'}$, displacement continuity $\widehat{\underline{W}}_E = \widehat{\underline{W}}_{E'}$ and force equilibrium $\widehat{\underline{F}}_E + \widehat{\underline{F}}_{E'} = 0$ have to be verified. By taking into account the search directions, the following explicit expressions are obtained:

$$\begin{cases} \widehat{\underline{W}}_E = \frac{1}{2}(\underline{W}_E + \underline{W}_{E'} - \boldsymbol{k}^{-1}(\underline{F}_E + \underline{F}_{E'})) \\ \widehat{\underline{F}}_E = \underline{F}_E + \boldsymbol{k}(\widehat{\underline{W}}_E - \underline{W}_E) \\ \widehat{\underline{W}}_{E'} = \widehat{\underline{W}}_E \\ \widehat{\underline{F}}_{E'} = -\widehat{\underline{F}}_E \end{cases} \tag{A.3}$$

■ **Frictional contact interfaces**

For frictional contact interfaces, here small displacements are assumed, which greatly simplifies contact pairing as well as the integration of the frictional contact conditions. At a contact interface $\Gamma_{EE'}$ between substructure Ω_E and $\Omega_{E'}$, Signorini non penetration conditions for the normal contact and Coulomb's law for the tangential frictional behavior [3, 4] have to be satisfied at the current time step t_j, as well as the interface force equilibrium. For the normal contact, the following conditions have to be verified:

$$\begin{cases} \underline{n} \cdot \widehat{\underline{W}}^{(j)}_{EE'} + g \geq 0 \;\Rightarrow \text{non penetration condition} \\ \underline{n} \cdot \widehat{\underline{F}}^{(j)}_{E} \leq 0 \;\Rightarrow \text{compressive contact force} \\ (\underline{n} \cdot \widehat{\underline{W}}^{(j)}_{EE'} + g)(\underline{n} \cdot \widehat{\underline{F}}^{(j)}_{E}) = 0 \;\Rightarrow \text{complementarity condition} \end{cases} \tag{A.4}$$

with g being the initial normal gap and $\underline{n}$ the outward normal from E to E'. For the tangential contact, a formulation in displacement increment is considered [32, 35]:

$$\begin{cases} \text{if } \|\Pi\widehat{\underline{F}}^{(j)}_{E}\| < f|\underline{n} \cdot \widehat{\underline{F}}^{(j)}_{E}| \;\Rightarrow \text{sticking} : \Pi\Delta\widehat{\underline{W}}^{(j)}_{EE'} = \underline{0} \\ \text{if } \|\Pi\widehat{\underline{F}}^{(j)}_{E}\| = f|\underline{n} \cdot \widehat{\underline{F}}^{(j)}_{E}| \;\Rightarrow \text{sliding} : \Pi\Delta\widehat{\underline{W}}^{(j)}_{EE'} = -\rho\Pi\widehat{\underline{F}}^{(j)}_{E}, \;\text{ with } \rho > 0 \end{cases} \tag{A.5}$$

In the previous equations, $\widehat{\underline{W}}^{(j)}_{EE'} = \widehat{\underline{W}}^{(j)}_{E'} - \widehat{\underline{W}}^{(j)}_{E}$ is the displacement jump at the interface, $\Delta\widehat{\underline{W}}^{(j)}_{EE'} = \widehat{\underline{W}}^{(j)}_{EE'} - \widehat{\underline{W}}^{(j-1)}_{EE'}$ is the increment of displacement jump between time step t_j and t_{j-1}, and f is the friction coefficient of the interface. Π is the projector on the tangential plane of the interface. The contact conditions are detected by means of proper contact indicators for the normal and tangential status. They are defined on unknown quantities of the local stage, and, by making use of the search directions, they can be equivalently written in terms of known quantities of the previous linear stage. Normal contact indicator C_N, and tangential sliding indicator $\underline{G}_T$ at the current time step are defined as follows:

$$\begin{cases} C^{(j)}_N := \frac{\boldsymbol{k}}{2}\widehat{\underline{W}}^{(j)}_{EE'} \cdot \underline{n} + \frac{\boldsymbol{k}}{2}g - \frac{1}{2}(\widehat{\underline{F}}^{(j)}_{E'} - \widehat{\underline{F}}^{(j)}_{E}) \cdot \underline{n} = \frac{\boldsymbol{k}}{2}(\underline{W}^{(j)}_{EE'}) \cdot \underline{n} + \frac{\boldsymbol{k}}{2}g - \frac{1}{2}(\underline{F}^{(j)}_{E'} - \underline{F}^{(j)}_{E}) \cdot \underline{n} \\ \underline{G}^{(j)}_T := \frac{\boldsymbol{k}}{2}\Pi\Delta\widehat{\underline{W}}^{(j)}_{EE'} - \frac{1}{2}\Pi(\widehat{\underline{F}}^{(j)}_{E'} - \widehat{\underline{F}}^{(j)}_{E}) = \frac{\boldsymbol{k}}{2}\Pi(\underline{W}^{(j)}_{EE'} - \widehat{\underline{W}}^{(j-1)}_{EE'}) - \frac{1}{2}\Pi(\underline{F}^{(j)}_{E'} - \underline{F}^{(j)}_{E}) \end{cases} \tag{A.6}$$

It should be noted that the evaluation of the tangential contact indicator at time t_j requires to know the solution of the local stage at time t_{j-1}. For this reason, the local stage has to be solved incrementally along the time steps. Once the contact indicator has been evaluated, contact forces are updated accordingly, as shown in **Table A.4**.

Subsequently, interface displacements are found explicitly with the search direction equations: $\widehat{\underline{W}}^{(j)}_E = \underline{W}^{(j)}_E + \boldsymbol{k}^{-1}(\widehat{\underline{F}}^{(j)}_E - \underline{F}^{(j)}_E)$ and $\widehat{\underline{W}}^{(j)}_{E'} = \underline{W}^{(j)}_{E'} + \boldsymbol{k}^{-1}(\widehat{\underline{F}}^{(j)}_{E'} - \underline{F}^{(j)}_{E'})$. The verification of contact conditions in the local stage of the LATIN is therefore completely explicit and does not require to solve a local nonlinear problem. It can be shown that contact forces and displacements satisfy contact conditions of Eq. (A.4) and Eq. (A.5), as well as the equilibrium of forces.

Normal contact	
■ **open contact:** $C_N^{(j)} > 0$	■ **closed contact:** $C_N^{(j)} \leqslant 0$
$\widehat{\underline{F}}_E^{(j)} = \widehat{\underline{F}}_{E'}^{(j)} = \underline{0}$	$\widehat{\underline{F}}_E^{(j)} \cdot \underline{n} = -\widehat{\underline{F}}_{E'}^{(j)} \cdot \underline{n} = C_N^{(j)}$
Tangential contact: if $C_N^{(j)} \leqslant 0$	
■ **sticking:** $\|\underline{G}_T^{(j)}\| < f\|\underline{n} \cdot \widehat{\underline{F}}_E^{(j)}\|$	■ **sliding:** $\|\underline{G}_T^{(j)}\| \geqslant f\|\underline{n} \cdot \widehat{\underline{F}}_E^{(j)}\|$
$\Pi\widehat{\underline{F}}_E^{(j)} = -\Pi\widehat{\underline{F}}_{E'}^{(j)} = \underline{G}_T^{(j)}$	$\Pi\widehat{\underline{F}}_E^{(j)} = -\Pi\widehat{\underline{F}}_{E'}^{(j)} = -fC_N^{(j)}\underline{G}_T^{(j)}/\|\underline{G}_T^{(j)}\|$

Table A.4: Resolution of the local stage for a frictional contact interface.

Appendix B. Downsizing stage

Here, the downsizing stage of the LATIN-PGD+D strategies is reported. The downsizing stage is performed on each substructure Ω_E and the downsizing algorithm [35] operates on the current basis $\{\underline{L}_k, \lambda_k\}_{k=1}^p$ of auxiliary mixed modes and time modes. Here $\langle\square,\square\rangle_{[0,T]}$ indicates $\int_{[0,T]} \square \cdot \square \mathrm{d}t$ and $\langle\square,\square\rangle_{\partial\Omega_E}$ stands for $\int_{\partial\Omega_E} \square \cdot \square \mathrm{d}S$. The associated norms are respectively $\|\square\|_{[0,T]}$ and $\|\square\|_{\partial\Omega_E}$.

Algorithm 3: Downsizing stage

for each substructure Ω_E **do**
- ■ **input**:
- – current basis of size p: $\{\underline{L}_k, \lambda_k\}_{k=1}^p$
- – relative amplitude cut-off: ϵ
- ■ **output:**
- – downsized basis of size $q \leqslant p$: $\{\underline{L}_m, \lambda_m\}_{m=1}^q$
- ■ **downsizing algorithm [35]:**
- **for** $n = 1$ *to* $n_{\max}$ **do**
  - – sort modes such that $\|\lambda_1\|_{[0,T]} \geqslant \cdots \geqslant \|\lambda_p\|_{[0,T]}$
  - **for** $i = p$ *down to* 2 **do**
    - **for** $j = 1$ *to* $i-1$ **do**
      - – project time mode: $\alpha = \langle\lambda_j, \lambda_i\rangle_{[0,T]}/\langle\lambda_j, \lambda_j\rangle_{[0,T]}$
      - – update corresponding space mode: $\underline{L}_j \leftarrow \underline{L}_j + \alpha\underline{L}_i$
      - – substract projected component: $\lambda_i \leftarrow \lambda_i - \alpha\lambda_j$
      - – project space mode: $\beta = \langle\underline{L}_j, \underline{L}_i\rangle_{\partial\Omega_E}/\langle\underline{L}_j, \underline{L}_j\rangle_{\partial\Omega_E}$
      - – update corresponding time mode: $\lambda_j \leftarrow \lambda_j + \beta\lambda_j$
      - – substract projected component: $\underline{L}_i \leftarrow \underline{L}_i - \beta\underline{L}_j$
      - – normalize $\underline{L}_j \leftarrow \underline{L}_j/\|\underline{L}_j\|_{\partial\Omega_E}$ and update $\lambda_j \leftarrow \lambda_j\|\underline{L}_j\|_{\partial\Omega_E}$
    - – normalize $\underline{L}_i \leftarrow \underline{L}_i/\|\underline{L}_i\|_{\partial\Omega_E}$ and update $\lambda_i \leftarrow \lambda_i\|\underline{L}_i\|_{\partial\Omega_E}$
  - **for** $i = p$ *down to* 1 **do**
    - **if** $\|\lambda_i\|_{[0,T]} < \epsilon\|\lambda_1\|_{[0,T]}$ **then**
      - – eliminate $\underline{L}_i$ and λ_i
      - – decrease basis size: $p \leftarrow p-1$
  - – set $q = p$

Acknowledgements

The authors acknowledge the financial support of ENS Paris-Saclay and IFP Energies nouvelles.

References

[1] Y. Estrin, Y. Beygelzimer, R. Kulagin, Design of architectured materials based on mechanically driven structural and compositional patterning, Advanced Engineering Materials 21 (9) (2019) 1900487.
[2] F. Bussolati, P.-A. Guidault, M. L. E. Guiton, O. Allix, P. Wriggers, Robust contact and friction model for the fatigue estimate of a wire rope in the mooring line of a floating offshore wind turbine, Lecture Notes in Application and Computational Mechanics 93 (2020) 249–270.
[3] P. Wriggers, T. A. Laursen, Computational Contact Mechanics, Vol. 2, Springer, 2006.
[4] V. Yastrebov, Computational contact mechanics: geometry, detection and numerical techniques, Ph.d. thesis, École Nationale Supérieure des Mines de Paris (2011).
[5] W. Hackbusch, Multi-grid methods and applications, Vol. 4, Springer Science & Business Media, 2013.
[6] P. Alart, F. Lebon, Solution of frictional contact problems using ILU and coarse/fine preconditioners, Computational Mechanics 16 (2) (1995) 98–105.
[7] F. Lebon, M. Raous, I. Rosu, Multigrid methods for unilateral contact problems with friction, in: IUTAM Symposium on Computational Methods in Contact Mechanics, Springer, 2007, pp. 1–16.
[8] P. Gosselet, C. Rey, Non-overlapping domain decomposition methods in structural mechanics, Archives of Computational Methods in Engineering 13 (4) (2006) 515–572.
[9] C. Farhat, F.-X. Roux, A method of finite element tearing and interconnecting and its parallel solution algorithm, International Journal for Numerical Methods in Engineering 32 (6) (1991) 1205–1227.
[10] C. Farhat, P.-S. Chen, F.-X. Roux, The dual Schur complement method with well-posed local Neumann problems: regularization with a perturbed Lagrangian formulation, SIAM Journal on Scientific Computing 14 (3) (1993) 752–759.
[11] C. Farhat, Implicit parallel processing in structural mechanics, Computational Mechanics Advances 2 (1994) 1–124.
[12] C. Farhat, J. Mandel, F. X. Roux, Optimal convergence properties of the FETI domain decomposition method, Computer Methods in Applied Mechanics and Engineering 115 (3-4) (1994) 365–385.
[13] D. Dureisseix, C. Farhat, A numerically scalable domain decomposition method for the solution of frictionless contact problems, International Journal for Numerical Methods in Engineering 50 (12) (2001) 2643–2666.
[14] Z. Dostál, F. A. G. Neto, S. A. Santos, Duality-based domain decomposition with natural coarse-space for variational inequalities, Journal of Computational and Applied Mathematics 126 (1-2) (2000) 397–415.
[15] Z. Dostál, F. A. G. Neto, S. A. Santos, Solution of contact problems by FETI domain decomposition with natural coarse space projections, Computer Methods in Applied Mechanics and Engineering 190 (13-14) (2000) 1611–1627.
[16] Z. Dostál, D. Horák, D. Stefanica, A scalable FETI-DP algorithm for a semi-coercive variational inequality, Computer Methods in Applied Mechanics and Engineering 196 (8) (2007) 1369–1379.
[17] Z. Dostál, D. Horák, D. Stefanica, A scalable FETI-DP algorithm with non-penetration mortar conditions on contact interface, Journal of Computational and Applied Mathematics 231 (2) (2009) 577–591.
[18] J. Dobiáš, S. Pták, Z. Dostál, V. Vondrák, Total FETI based algorithm for contact problems with additional non-linearities, Advances in Engineering Software 41 (1) (2010) 46–51.
[19] P. Ladevèze, Nonlinear Computational Structural Mechanics - new approaches and non-incremental methods of calculation, Mechanical Engineering Series, Springer New York, 1999.
[20] L. Champaney, J.-Y. Cognard, P. Ladevèze, Modular analysis of assemblages of three-dimensional structures with unilateral contact conditions, Computers & Structures 73 (1-5) (1999) 249–266.
[21] P. Oumaziz, P. Gosselet, P.-A. Boucard, S. Guinard, A non-invasive implementation of a mixed domain decomposition method for frictional contact problems, Computational Mechanics 60 (2017) 797–812.
[22] P. Ladevèze, O. Loiseau, D. Dureisseix, A micro-macro and parallel computational strategy for highly heterogeneous structures, International Journal for Numerical Methods in Engineering 52 (1-2) (2001) 121–138.
[23] P. Ladevèze, A. Nouy, O. Loiseau, A multiscale computational approach for contact problems, Computer Methods in Applied Mechanics and Engineering 191 (43) (2002) 4869–4891.
[24] J. S. Hesthaven, G. Rozza, B. Stamm, Certified reduced basis methods for parametrized partial differential equations, Vol. 590, Springer, 2016.
[25] F. Chinesta, P. Ladeveze, E. Cueto, A short review on model order reduction based on proper generalized decomposition, Archives of Computational Methods in Engineering 18 (4) (2011) 395–404.
[26] A. Chatterjee, An introduction to the proper orthogonal decomposition, Current Science (2000) 808–817.
[27] G. Rozza, D. B. P. Huynh, A. T. Patera, Reduced basis approximation and a posteriori error estimation for affinely parametrized elliptic coercive partial differential equations, Archives of Computational Methods in Engineering 15 (3) (2008) 229–275.
[28] A. Nouy, A priori model reduction through proper generalized decomposition for solving time-dependent partial differential equations, Computer Methods in Applied Mechanics and Engineering 199 (23-24) (2010) 1603–1626.
[29] M. Balajewicz, D. Amsallem, C. Farhat, Projection-based model reduction for contact problems, International Journal for Numerical Methods in Engineering 106 (8) (2016) 644–663.
[30] A. Benaceur, A. Ern, V. Ehrlacher, A reduced basis method for parametrized variational inequalities applied to contact mechanics, International Journal for Numerical Methods in Engineering 121 (6) (2020) 1170–1197.
[31] M. Barrault, Y. Maday, N. C. Nguyen, A. T. Patera, An 'empirical interpolation' method: application to efficient reduced-basis discretization of partial differential equations, Comptes Rendus Mathématique 339 (9) (2004) 667–672.

[32] R. A. Cardoso, D. Néron, S. Pommier, J. A. Araújo, An enrichment-based approach for the simulation of fretting problems, Computational Mechanics 62 (6) (2018) 1529–1542.
[33] I. Niakh, G. Drouet, V. Ehrlacher, A. Ern, Stable model reduction for linear variational inequalities with parameter-dependent constraints, ESAIM: Mathematical Modelling and Numerical Analysis 57 (1) (2023) 167–189.
[34] K. S. Kollepara, J. M. Navarro-Jiménez, Y. Le Guennec, L. Silva, J. V. Aguado, On the limitations of low-rank approximations in contact mechanics problems, International Journal for Numerical Methods in Engineering 124 (1) (2023) 217–234.
[35] A. Giacoma, D. Dureisseix, A. Gravouil, M. Rochette, Toward an optimal a priori reduced basis strategy for frictional contact problems with LATIN solver, Computer Methods in Applied Mechanics and Engineering 283 (2015) 1357–1381.
[36] A. Giacoma, D. Dureisseix, A. Gravouil, M. Rochette, A multiscale large time increment/FAS algorithm with time-space model reduction for frictional contact problems, International Journal for Numerical Methods in Engineering 97 (3) (2014) 207–230.
[37] P.-A. Guidault, D. Zeka, D. Néron, M. Guiton, G. Enchéry, Model order reduction for the fatigue life prediction of wire ropes in tension and bending, in: 7th International Conference on Computational Contact Mechanics, 2023.
[38] M. Cremonesi, D. Néron, P.-A. Guidault, P. Ladevèze, A PGD-based homogenization technique for the resolution of nonlinear multiscale problems, Computer Methods in Applied Mechanics and Engineering 267 (2013) 275–292.
[39] P. Ladevèze, J.-C. Passieux, D. Néron, The LATIN multiscale computational method and the proper generalized decomposition, Computer Methods in Applied Mechanics and Engineering 199 (21-22) (2010) 1287–1296.
[40] P. Ladevèze, D. Néron, P. Gosselet, On a mixed and multiscale domain decomposition method, Computer Methods in Applied Mechanics and Engineering 196 (8) (2007) 1526–1540.
[41] A. Nouy, P. Ladevèze, Multiscale computational strategy with time and space homogenization: a radial-type approximation technique for solving microproblems, International Journal for Multiscale Computational Engineering 2 (4) (2004).
[42] A. Caignot, P. Ladèveze, D. Néron, J.-F. Durand, Virtual testing for the prediction of damping in joints, Engineering Computations 27 (5) (2010) 621–644.
[43] P. Kerfriden, O. Allix, P. Gosselet, A three-scale domain decomposition method for the 3d analysis of debonding in laminates, Computational mechanics 44 (3) (2009) 343–362.
[44] K. Saavedra, O. Allix, P. Gosselet, On a multiscale strategy and its optimization for the simulation of combined delamination and buckling, International Journal for Numerical Methods in Engineering 91 (7) (2012) 772–798.
[45] P.-A. Guidault, O. Allix, L. Champaney, C. Cornuault, A multiscale extended finite element method for crack propagation, Computer Methods in Applied Mechanics and Engineering 197 (5) (2008) 381–399.
[46] G. H. Golub, C. Reinsch, Singular value decomposition and least squares solutions, Linear algebra 2 (1971) 134–151.
[47] P.-E. Allier, L. Chamoin, P. Ladevèze, Proper generalized decomposition computational methods on a benchmark problem: introducing a new strategy based on constitutive relation error minimization, Advanced Modeling and Simulation in Engineering Sciences 2 (1) (2015) 1–25.
[48] R. Glowinski, P. Le Tallec, Augmented Lagrangian and operator-splitting methods in nonlinear mechanics, SIAM, 1989.
[49] R. Glowinski, P. Le Tallec, Augmented lagrangian interpretation of the nonoverlapping schwarz alternating method, in: Third international symposium on domain decomposition methods for partial differential equations, 1990, pp. 224–231.
[50] R. Glowinski, Augmented Lagrangians and Alternating Direction Methods of Multipliers, Society for Industrial and Applied Mathematics, 2015, Ch. 4, pp. 157–202.
[51] M. Fortin, R. Glowinski, Augmented Lagrangian methods: applications to the numerical solution of boundary-value problems, Elsevier, 2000.
[52] J. C. Simo, T. Laursen, An augmented lagrangian treatment of contact problems involving friction, Computers and Structures 42 (1) (1992) 97–116.
[53] J. C. Passieux, P. Ladevèze, D. Néron, A scalable time–space multiscale domain decomposition method: adaptive time scale separation, Computational Mechanics 46 (4) (2010) 621–633.
[54] A. R. Cardoso, Numerical studies on the modeling of fretting fatigue (in french), Ph.D. thesis, Université Paris-Saclay (2019).
[55] R. Ribeaucourt, M.-C. Baietto-Dubourg, A. Gravouil, A new fatigue frictional contact crack propagation model with the coupled X-FEM/LATIN method, Computer Methods in Applied Mechanics and Engineering 196 (33-34) (2007) 3230–3247.
[56] P. Ladevèze, A. Nouy, On a multiscale computational strategy with time and space homogenization for structural mechanics, Computer Methods in Applied Mechanics and Engineering 192 (28-30) (2003) 3061–3087.
[57] A. Nouy, A multiscale strategy with homogenization in space and time for highly heterogeneous structures (in french), Ph.D. thesis, École normale supérieure de Cachan (2003).
[58] S. Alameddin, A. Fau, D. Néron, P. Ladevèze, U. Nackenhorst, Toward optimality of proper generalised decomposition bases, Mathematical and Computational Applications 24 (1) (2019) 30.
[59] M. Brand, Fast low-rank modifications of the thin singular value decomposition, Linear Algebra and its Applications 415 (1) (2006) 20–30.
[60] J. R. Bunch, C. P. Nielsen, Updating the singular value decomposition, Numerische Mathematik 31 (2) (1978) 111–129.
[61] M. Pastor, M. Binda, T. Harčarik, Modal assurance criterion, Procedia Engineering 48 (2012) 543–548.
[62] P. Ladevèze, D. Dureisseix, A micro/macro approach for parallel computing of heterogeneous structures, International Journal for Computational Civil and Structural Engineering 1 (2000) 18–28.
[63] P. M. Mariano, Multifield theories in mechanics of solids, Advances in Applied Mechanics 38 (2002) 1–93.
[64] S. Montalvo, S. Fouvry, M. Martinez, A hybrid analytical-FEM 3D approach including wear effects to simulate fretting fatigue endurance: application to steel wires in crossed contact, Tribology International (2023) 108713.
[65] M. Capaldo, P.-A. Guidault, D. Néron, P. Ladevèze, The reference point method, a "hyperreduction" technique: Application to PGD-based nonlinear model reduction, Computer Methods in Applied Mechanics and Engineering 322 (2017) 483–514.